Chemical Geology 262 (2009) 229–245

Contents lists available at ScienceDirect

Chemical Geology

journal homepage: www.elsevier.com/locate/chemgeo

Zircon U–Pb geochronology and Hf isotopic constraints on petrogenesis of the Gangdese batholith, southern Tibet

Wei-Qiang Ji [a], Fu-Yuan Wu [a,*], Sun-Lin Chung [b], Jin-Xiang Li [a], Chuan-Zhou Liu [a]

[a] State Key Laboratory of Lithospheric Evolution, Institute of Geology and Geophysics, Chinese Academy of Sciences, P.O. Box 9825, Beijing 100029, China
[b] Department of Geosciences, National Taiwan University, Taipei 106, Taiwan

ARTICLE INFO

Article history:
Received 16 June 2008
Received in revised form 16 January 2009
Accepted 20 January 2009

Editor: R.L. Rudnick

Keywords:
U–Pb age
Hf isotope
Zircon
Gangdese batholith
Petrogenesis
Tibet

ABSTRACT

During the Mesozoic–Cenozoic, northward Neotethyan subduction and subsequent India–Asia collision gave rise to the extensive Transhimalayan magmatism that stretches from Burma and western Yunnan through southern Tibet to the Ladakh and Kohistan complexes. To understand the age distribution and petrogenesis of the Gangdese batholith, the largest intrusive exposure along the Transhimalayan magmatic belt, fifty granitic samples were selected for *in situ* zircon U–Pb and Hf isotopic analyses. The U–Pb data suggest four discrete stages of magmatic activity, i.e., ~205–152, ~109–80, ~65–41 and ~33–13 Ma, respectively, with the 65–41 Ma stage being the most prominent. The Hf isotopic data indicate that the Gangdese batholith is overwhelmed by positive $\varepsilon_{Hf}(t)$ values, which are comparable to those of the Kohistan–Ladakh batholiths in the west but differ markedly from those of the Chayu–Burma batholiths in the east. Most of the Gangdese granites show similar and young Hf model ages (1000–300 Ma), indicating their derivation from juvenile crust. However, those formed in the 65–41 Ma stage exhibit more heterogeneous Hf isotopic ratios, with negative $\varepsilon_{Hf}(t)$ values being observed in some granites younger than 50 Ma, suggesting the involvement of old Indian continental crust in their petrogenesis. This age may thus mark the onset of the India–Asia collision. The newly established zircon U–Pb age and Hf isotope database of the Gangdese batholith can be used as a powerful tracer or "fingerprint" when studying the source-to-sink relation of the sediments eroded from the southern Tibetan Plateau.

1. Introduction

Granite is a major constituent of the continental crust. The petrogenesis of the granite is, therefore, vital to studying the growth and evolution of the continents. It was generally thought that granites are derived from the partial melting of pre-existed crustal materials, as indicated by the low Nd isotopic ($^{143}Nd/^{144}Nd$) ratios and old Nd model ages (e.g., Allègre and Ben Othman, 1980). However, many granites show high Nd isotopic ratios and young Nd model ages, suggesting their derivations from either recycling of juvenile crust or nascent mantle input to the continental crust (cf. Jahn et al., 2000).

In Tibet, during oceanic closure, terrane amalgamation and/or collision, and subsequent post-orogenic processes between India and Asia, various kinds of granites were formed (Le Fort, 1988) (Fig. 1). The most characterized granites in the region is the Transhimalayan batholith, exposed along the southern margin of the Lhasa terrane and extended from the Kohistan–Ladakh batholith in the west through Gangdese batholith in the middle to the Chayu–western Yunnan (Dianxi) –Burma batholith in the east, with a length of > 3000 km (Fig. 1). Although this gigantic batholith has attracted much academic attention over the past decades, its geochronological framework, petrogenesis and relationship with Tethysan ocean closure and India–Asia collision remains unclear. In terms of geochronology, the pioneering work by Schärer et al. (1984a,b) indicate that the Gangdese batholith, the largest individual body in the Transhimalayan batholith, was largely emplaced in the Paleocene–Eocene and subordinately in the Cretaceous, a notion that was supported by subsequent studies (Harrison et al., 2000; McDermid et al., 2002; Dong et al., 2005; Mo et al., 2005a,b; Xia et al., 2007; Wen et al., 2008). However, recent data indicate that older (Jurassic) and younger (Oligo–Miocene) magmatic activities were more widely developed in the Gangdese belt than previously thought (cf. Chung et al., 2005). The Jurassic granites, exposed in localities with zircon U–Pb ages dated at 188–178 Ma (Chu et al., 2006; Zhang et al., 2007a; Yang et al., 2008b) and somewhat deformed in the field, have geochemical compositions that suggest an origin related to northward subduction of the Neotethyan oceanic slab under Asia. The Oligo–Miocene granites, dominated with porphyritic texture and bearing giant copper deposits (Hou et al., 2004), have been dated at 30–10 Ma (Chung et al., 2003, Hou et al., 2004; Guo et al., 2007) that postdates the India–Asia collision starting sometime around 70–35 Ma (cf. Yin and Harrison

* Corresponding author. Tel.: +86 10 82998217; fax: +86 10 62010846.
E-mail address: wufuyuan@mail.igcas.ac.cn (F.-Y. Wu).

0009-2541/$ – see front matter © 2009 Elsevier B.V. All rights reserved.
doi:10.1016/j.chemgeo.2009.01.020

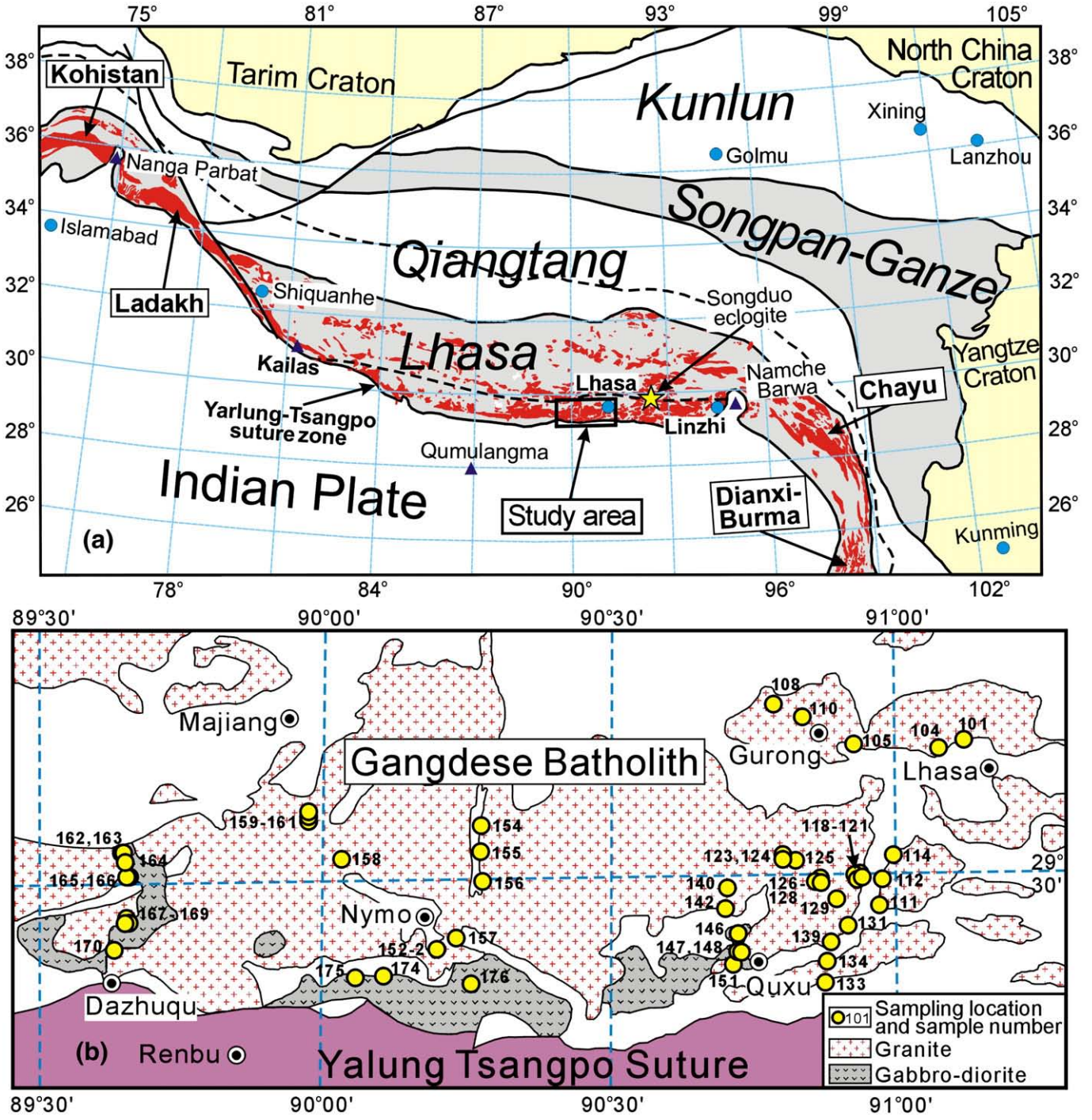

Fig. 1. (a) Distribution map of the Transhimalayan batholith. The dash line marks the boundary between the south and north Lhasa terranes, along which the Songduo eclogite is indicated; (b) Detailed occurrences of granites from Lhasa–Dazhuqu sections of the Gangdese batholith with sampling locations. The number beside the yellow circle indicates the last three digits of the sample (e.g., 108 means 06FW108). (For interpretation of the references to colour in this figure legend, the reader is referred to the web version of this article.)

(2000) and Aitchison et al. (2007); for detailed reviews) and therefore is petrogenetically unrelated to the pre-collisional Neotethyan subduction.

Furthermore, studies have repeatedly shown that the Gangdese batholith is characterized by low initial $^{87}Sr/^{86}Sr$ (~0.705), coupled with high and positive $\varepsilon_{Nd}(t)$ (+4.9 to +2.5) and $\varepsilon_{Hf}(t)$ (+10 to +18) values, yielding young Nd and Hf model ages of 0.4–0.7 Ga (Harris et al., 1988; Jiang et al., 1999; Mo et al., 2005a; Chung et al., 2005; Chu et al., 2006; Zhang et al., 2007a). The overall isotopic features, reflecting a juvenile nature of the magma source similar to that observed in the Phanerozoic granites from the Central Asian Orogenic Belt (Jahn et al., 2000), require the formation of these granites either by partial melting of the subducted oceanic crust and/or underplated mafic material from the depleted mantle, or by mixing between the mafic and felsic magmas. Therefore, we conducted a detailed zircon U–Pb "age mapping" study of the Gangdese batholith. Zircon *in situ* Hf isotopic analysis was also performed to better constrain the petrogenetic processes involved. Lastly, we combined our comprehensive database with relevant information to explore the pre- to post-collisional geodynamic evolution in southern Tibet for a long period of time from the early Mesozoic to late Cenozoic.

2. Geological background and samples

The Tibetan plateau is geologically composed of the Indian continent in the south and the Asian continent in the north, separated by the Yarlung–Tsangpo suture zone (Fig. 1a). South of the suture zone lies the Tethyan Himalaya, consisting of low-grade metasedimentary and sedimentary rocks of Cambrian–Eocene ages that were originally deposited along the passive margin of northern India (Allègre et al., 1984; Yin and Harrison, 2000). Within the Tethyan Himalaya Precambrian–Cambrian granites crop out in a series of metamorphic core complexes, often associated with leucogranites that were emplaced at ~30–10 Ma (Schärer et al., 1986; Zhang et al., 2004). Cretaceous to Lower Tertiary marine sedimentary sequences are locally preserved (Willems et al., 1996; Ding, 2003, Ding et al., 2005; Zhu et al., 2005; Li et al., 2005). To further south, separating by the South Tibetan Detachment Zone and then the Main Central Thrust, there exist the High and Lesser Himalayas, respectively. The High Himalaya is mainly composed of amphibolite-facies Proterozoic metasedimentary rocks, intruded locally by early Paleozoic granites (Lee et al., 2000; Gehrels et al., 2003). North of the Yarlung–Tsangpo suture zone, the Lhasa terrane that represents the southernmost part of the Asian continent is characterized by extensive Jurassic–Early Tertiary calc-alkaline granitoids (Debon et al., 1986; Chung et al., 2005; Wen et al., 2008) and Cretaceous to Tertiary terrestrial volcanic sequences of the Linzizong Formation (Maluski et al., 1982; Coulon et al., 1986; Chung et al., 2005; Zhou et al., 2004; He et al., 2007; Lee et al., 2007; Mo et al., 2003, 2007, 2008). Further northward, the Qiangtang terrane is juxtaposed with the Lhasa terrane along the Bangong–Nujiang suture zone that closed during the Middle Jurassic to Early Cretaceous (Allègre et al., 1984; Kapp et al., 2005).

As a prominent part of the Transhimalaya batholith, the Gangdese batholith is located in southern Tibet and extended from Kailas in the west through Lhasa, and then to Linzhi in the east (Fig. 1a). The major Gangdese rock types include gabbro, diorite, granodiorite, monzogranite and/or syenogranite. Except for gabbro, which contains orthopyroxene, clinopyroxene and various contents of amphiboles, all these rocks are coarse-grained with mineral assemblage of quartz, plagioclase, potassium feldspar, biotite and hornblende, indicating that the granites genetically belong to I-type granites. Field investigations suggest that phenocrysts of potassium feldspar are common for the granodiorite and

Table 1
Summary of zircon U–Pb ages and Hf isotopic compositions of the Gangdese batholith.

Sample	Location	GPS position	Section	Rock type	Age (Ma)	$\varepsilon_{Hf}(t)$	T_{DM2} (Ma)
06FW101	North of Lhasa	N29°41′12″, E91°06′42″	Lhasa	Bi-monzogranite	64.7 ± 1.1	7.9 ± 0.3	873 ± 30
06FW104	North of Lhasa	N29°40′31″, E91°04′32″	Lhasa	Bi-monzogranite	64.4 ± 0.9	6.9 ± 0.8	949 ± 63
06FW105	Yangda	N29°40′54″, E90°55′55″	Lhasa	Bi-monzogranite	55.2 ± 1.5	6.0 ± 0.4	1018 ± 36
06FW108	North of Gurong	N29°45′32″, E90°46′32″	Lhasa	Hb-Bi-granodiorite	56.8 ± 0.7	7.7 ± 0.5	858 ± 38
06FW110	Zhongduiguo	N29°44′15″, E90°49′59″	Lhasa	Bi-monzogranite	54.3 ± 0.9	7.7 ± 0.4	872 ± 30
06FW111	Caina	N29°26′36″, E90°57′23″	Quxu	Hb–Bi-monzogranite	50.6 ± 0.7	11.1 ± 0.4	566 ± 30
06FW112	North of Caina	N29°29′26″, E90°57′40″	Quxu	Hb-Bi-granodiorite	53.4 ± 1.0	10.6 ± 0.4	600 ± 30
06FW114	Northeast Caina	N29°31′51″, E90°59′35″	Quxu	Hb-Bi-granodiorite	86.4 ± 1.6	11.5 ± 0.5	552 ± 44
06FW118	Niedang	N29°29′57″, E90°56′19″	Quxu	Bi-monzogranite	51.0 ± 0.7	10.6 ± 0.5	600 ± 44
06FW119	Niedang	N29°29′57″, E90°56′19″	Quxu	Bi-granodiorite	51.2 ± 0.7	11.1 ± 0.4	530 ± 33
06FW120	Niedang	N29°29′57″, E90°56′19″	Quxu	Dioritic enclave	50.3 ± 0.6	10.9 ± 0.4	585 ± 37
06FW121	Niedang	N29°29′57″, E90°56′19″	Quxu	Granitic dike	51.1 ± 0.7	11.0 ± 1.0	553 ± 40
06FW123	Nanmu Copper	N29°31′18″, E90°48′38″	Quxu	Bi-monzogranite	17.0 ± 0.9	5.8 ± 0.7	1041 ± 44
06FW124	Nanmu Copper	N29°31′18″, E90°48′38″	Quxu	Granitic porphyrite	15.3 ± 0.4	6.9 ± 1.1	926 ± 97
06FW125	East of Nanmu Copper	N29°31′02″, E90°49′29″	Quxu	Hb-Bi-monzogranite	17.7 ± 0.6	6.4 ± 0.7	992 ± 39
06FW126	Nanmu Power Station	N29°28′54″, E90°52′26″	Quxu	Hb-granodiorite	55.3 ± 1.0	6.4 ± 0.7	989 ± 54
06FW127	Nanmu Power Station	N29°28′54″, E90°52′26″	Quxu	Granitic dike	49.5 ± 0.6	7.4 ± 0.3	915 ± 18
06FW128	Nanmu Power Station	N29°28′54″, E90°52′26″	Quxu	Doleritic dike	49.9 ± 1.0	9.4 ± 1.4	720 ± 130
06FW129	Nanmu	N29°27′50″, E90°53′48″	Quxu	Hb-Bi-granodiorite	52.9 ± 0.7	6.2 ± 0.6	1016 ± 53
06FW131	Jiangcun	N29°24′28″, E90°54′21″	Quxu	Tonalitic gneiss	44.0 ± 0.8	2.7 ± 1.2	1335 ± 110
06FW133	Galashan tunnel	N29°20′01″, E90°51′56″	Quxu	Bi-Hb-monzonite	47.1 ± 1.0	0.9 ± 0.6	1486 ± 38
06FW134	Galashan tunnel	N29°21′38″, E90°52′32″	Quxu	Bi-monzogranite	41.9 ± 0.6	2.3 ± 0.6	1367 ± 53
06FW139	East of Quxu	N29°22′59″, E90°42′56″	Quxu	Qz monzonite	41.5 ± 0.7	0.6 ± 0.5	1513 ± 38
06FW140	Badi	N29°28′21″, E90°42′56″	Quxu	Bi-monzogranite	43.7 ± 0.9	7.0 ± 2.0	915 ± 130
06FW142	Baijin	N29°26′21″, E90°42′39″	Quxu	Bi-monzogranite	21.3 ± 0.6	9.0 ± 0.9	817 ± 110
06FW146	Qupu	N29°24′10″, E90°43′03″	Quxu	Gabbro	56.9 ± 1.4	13.0 ± 0.3	402 ± 24
06FW147	Northwest of Quxu	N29°22′03″, E90°43′28″	Quxu	Bi-granodiorite	51.5 ± 0.8	13.4 ± 0.3	365 ± 24
06FW148	Northwest of Quxu	N29°22′03″, E90°43′28″	Quxu	Syenogranitic dike	51.3 ± 0.6	11.7 ± 0.5	508 ± 34
06FW151	West of Quxu	N29°21′27″, E90°43′00″	Quxu	Diorite	55.5 ± 1.2	12.7 ± 0.4	434 ± 31
06FW152-2	East of Qulin	N29°24′05″, E90°10′44″	Nymo	Diorite	57.3 ± 0.9	12.9 ± 0.4	410 ± 32
06FW154	Angang	N29°34′41″, E90°16′27″	Nymo	Bi-monzogranite	51.3 ± 0.7	8.2 ± 0.4	825 ± 30
06FW155	Angang Power Station	N29°32′33″, E90°16′23″	Nymo	Bi-monzogranite	61.1 ± 1.2	7.7 ± 0.7	899 ± 54
06FW156	Kongdonglang	N29°29′58″, E90°16′16″	Nymo	Bi-monzogranite	55.4 ± 0.8	8.5 ± 0.5	823 ± 40
06FW157	Northwest of Qulin	N29°24′49″, E90°13′24″	Nymo	Monzogranite	32.5 ± 0.5	5.0 ± 0.6	1105 ± 56
06FW158	Southwest of Nymo	N29°31′15″, E90°02′31″	Nymo	Bi-monzogranite	14.9 ± 0.3	4.7 ± 0.5	1133 ± 39
06FW159	Chongjiang Copper	N29°36′25″, E89°59′02″	Nymo	Monzogranite	15.3 ± 0.2	4.6 ± 0.5	1136 ± 42
06FW160	Chongjiang Copper	N29°36′25″, E89°59′02″	Nymo	Granitic porphyrite	13.7 ± 0.3	6.2 ± 1.0	997 ± 55
06FW161	Chongjiang Copper	N29°36′25″, E89°59′02″	Nymo	Dioritic porphyrite	13.5 ± 0.4	6.4 ± 0.6	948 ± 52
06FW174	Karu	N29°21′04″, E90°05′49″	Nymo	Hb-diorite	50.2 ± 1.5	10.9 ± 0.4	585 ± 35
06FW175	Karu	N29°20′56″, E90°04′02″	Nymo	Hb-quartz diorite	52.6 ± 1.2	11.2 ± 0.6	554 ± 44
06FW176	Nymo	N29°20′05″, E90°14′57″	Nymo	Hb-diorite	53.6 ± 1.0	11.3 ± 0.9	559 ± 63
06FW162	Numa	N29°32′20″, E89°37′21″	Dazhuqu	Granodiorite	50.9 ± 0.8	11.8 ± 0.6	552 ± 26
06FW163	Numa	N29°32′20″, E89°37′21″	Dazhuqu	Monzogranite	48.2 ± 0.7	11.0 ± 0.4	525 ± 35
06FW164	Numa	N29°31′19″, E89°37′24″	Dazhuqu	Monzogranite	184.9 ± 3.8	14.4 ± 0.5	376 ± 38
06FW165	North of Numa	N29°30′12″, E89°37′52″	Dazhuqu	Granodioritic gneiss	194.0 ± 3.5	15.3 ± 0.4	282 ± 35
06FW166	North of Numa	N29°30′12″, E89°37′52″	Dazhuqu	Monzogranitic gneiss	205.3 ± 3.0	14.8 ± 0.6	340 ± 34
06FW167	West of Numa	N29°26′23″, E89°37′55″	Dazhuqu	Monzogranite	155.9 ± 2.3	11.6 ± 0.5	592 ± 39
06FW168	West of Numa	N29°26′23″, E89°37′55″	Dazhuqu	Hb-diorite	174.2 ± 2.5	13.6 ± 0.7	431 ± 51
06FW169	West of Numa	N29°26′23″, E89°37′55″	Dazhuqu	Syenogranitic dike	151.8 ± 1.6	13.2 ± 0.6	444 ± 38
06FW170	North of Dazhuqu	N29°23′34″, E89°37′42″	Dazhuqu	Bi-Hb-diorite	108.6 ± 1.5	13.2 ± 0.4	416 ± 34

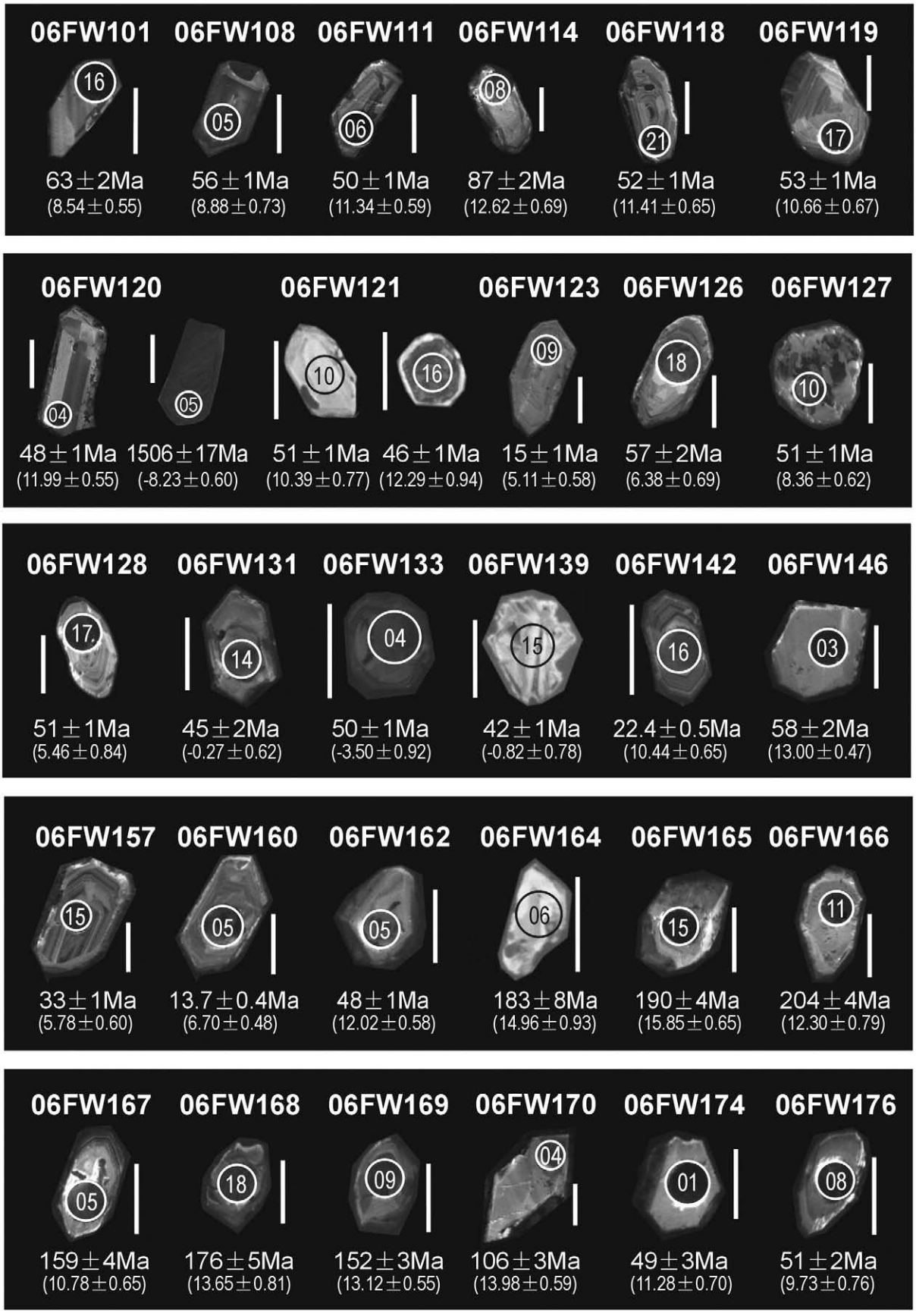

Fig. 2. Representative cathodoluminescence (CL) images of zircons from the Gangdese batholith with identified analytical number, U–Pb age and $\varepsilon_{Hf}(t)$ value (scale bar = 100 μm).

monzogranite. In some localities, amazonite-bearing alkali feldspar granite is also identified. In this study, we analyzed fifty granitic samples collected from the middle part of the Gangdese batholith, from Lhasa–Gurong, Quxu, Nymo and Dazhuqu areas, respectively (Fig. 1b).

3. Analytical methods

Zircon crystals were obtained from crushed rock using a combined method of heavy liquid and magnetic separation techniques. Individual crystals were hand picked and mounted in epoxy resin. Experiments were carried out at the MC-ICPMS laboratory of the Institute of Geology and Geophysics, Chinese Academy of Sciences. An Agilent 7500a quadruple (Q) -ICPMS and a Neptune multi-collector (MC)-ICPMS were used for simultaneous determination of zircon U–Pb age, trace elements and Lu–Hf isotopes with a 193 nm excimer ArF laser-ablation system (GeoLas Plus) attached. The detailed analytical procedures can be found in Xie et al. (2008), only an outline is given here.

Before analysis, the sample surface was cleaned with ethanol to eliminate possible contamination. Every 5 sample analyses were followed by analyzing of a suit of zircon standards, i.e., Harvard zircon 91500 (Wiedenbeck et al., 1995), Australian National University standard zircon TEMORA (Black et al., 2003) and NIST SRM 610. Each spot analysis consisted approximately of 30 s background acquisition and 40 s sample data acquisition. During experiments, the ablation material was sent to the Q-ICPMS and MC-ICPMS simultaneously for U–Pb and Hf isotopic analyses. $^{207}Pb/^{206}Pb$, $^{206}Pb/^{238}U$, $^{207}U/^{235}U$ ($^{235}U = {}^{238}U/137.88$), $^{208}Pb/^{232}Th$ ratios were corrected by using zircon 91500 as external standard. The fractionation correction and results were calculated using GLITTER 4.0 (Macquarie University) (Jackson et al., 2004). Common Pb was corrected according to the method proposed by Anderson (2002). The weighted mean U–Pb ages and concordia plots were processed using ISOPLOT 3.0 (Ludwig, 2003). For Hf analyses, the isobaric interference of ^{176}Lu on ^{176}Hf is negligible due to the extremely low $^{176}Lu/^{177}Hf$ in zircon (normally <0.002). The interference of ^{176}Yb on ^{176}Hf was calculated by measuring the mean $^{173}Yb/^{171}Yb$ ratio of the individual spot, and then calculating the fractionation coefficient of Yb, and finally deducting the contribution of ^{176}Yb to ^{176}Hf. assuming $^{176}Yb/^{172}Yb = 0.5887$. During this study of analyses, TEMORA 1 as an unknown sample yielded a weighted $^{206}Pb/^{238}U$ age of 416 ± 2 Ma ($2\sigma_m$, MSWD = 0.1, $n = 50$) and a weighted $^{176}Hf/^{177}Hf$ ratio of 0.282673 ± 0.000005 ($2\sigma_m$, MSWD = 4.0, $n = 50$), which is in good agreement with the recommended U–Pb age and Hf isotopic ratio (Black et al., 2003; Wu et al., 2006). During data acquisition of Hf isotopes, $^{176}Hf/^{177}Hf$ isotopic ratio of 0.282305 is recommended as the standard value for 91500 (Wu et al., 2006).

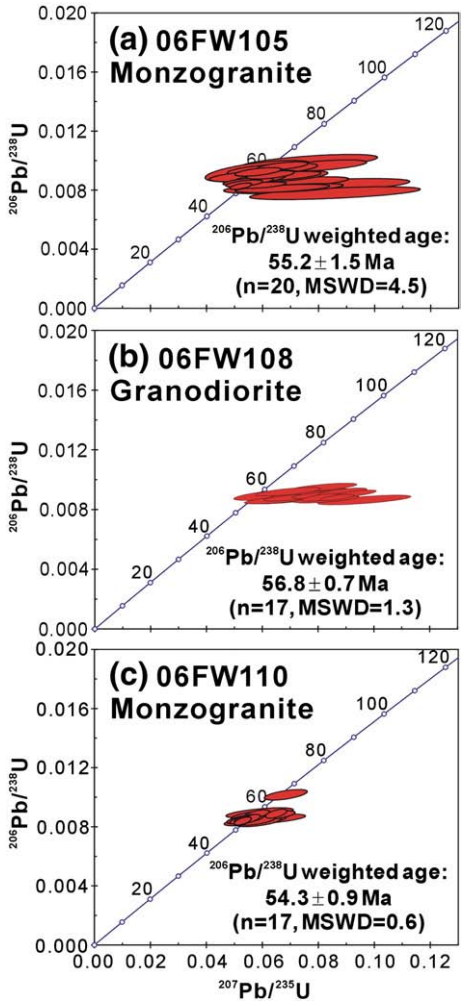

Fig. 4. Zircon U–Pb concordia diagrams of granites from the Gurong pluton in the Lhasa section (3 samples).

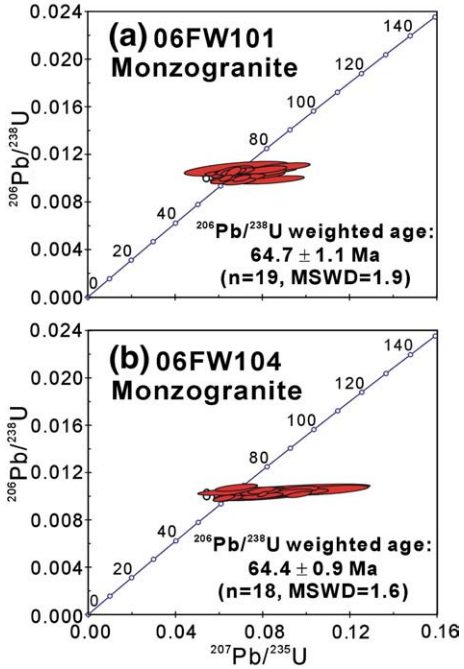

Fig. 3. Zircon U–Pb concordia diagrams of granites from Lhasa pluton in the Lhasa section (2 samples).

The notations of ε_{Hf}, $f_{Lu/Hf}$ and T_{Hf} in this study are defined as:

$$\varepsilon_{Hf(0)} = \left(\left(^{176}Hf/^{177}Hf\right)_s / \left(^{176}Hf/^{177}Hf\right)_{CHUR,0} - 1\right) \times 10000$$

$$\varepsilon_{Hf(t)} = \left(\left(^{176}Hf/^{177}Hf\right)_s - \left(^{176}Lu/^{177}Hf\right)_s \times \left(e^{\lambda t} - 1\right)\right) / \left(\left(^{176}Hf/^{177}Hf\right)_{CHUR,0} - \left(^{176}Lu/^{177}Hf\right)_{CHUR} \times \left(e^{\lambda t} - 1\right)\right) - 1 \times 10000$$

$$T_{Hf} = 1/\lambda \times \left(1 + \left(\left(^{176}Hf/^{177}Hf\right)_s - \left(^{176}Hf/^{177}Hf\right)_{DM}\right) / \left(\left(^{176}Lu/^{177}Hf\right)_s - \left(^{176}Lu/^{177}Hf\right)_{DM}\right)\right)$$

$$f_{Lu/Hf} = \left(^{176}Lu/^{177}Hf\right)_s / \left(^{176}Lu/^{177}Hf\right)_{CHUR} - 1$$

where, $(^{176}Lu/^{177}Hf)_S$ and $(^{176}Hf/^{177}Hf)_S$ are the measured values of samples, $(^{176}Lu/^{177}Hf)_{CHUR} = 0.0332$ and $(^{176}Hf/^{177}Hf)_{CHUR,0} = 0.282772$

(Blichert-Toft and Albarede, 1997); $(^{176}Lu/^{177}Hf)_{DM} = 0.0384$ and $(^{176}Hf/^{177}Hf)_{DM} = 0.28325$ (Griffin et al., 2000), t = crystallization time of zircon.

As for zircons crystallized from a crustal source, we also calculated two-stage Hf model ages (T_{Hf2}) using the same assumption as Keto and Jacobson (1987) for Nd isotopes:

$$T_{Hf2} = T_{Hf1} - (T_{Hf1} - t)((f_{LC} - f_s) / (f_{LC} - f_{DM}))$$

where, f_{LC}, f_s, $f_{DM} = f_{Lu/Hf}$ values of the crustal source, the sample and the depleted mantle, respectively. In our calculation, $f_{LC} = -0.34$ ($^{176}Lu/^{177}Hf = 0.22$ lower continental crust, Amelin et al. (1999)) and $f_{DM} = 0.157$ ($^{176}Lu/^{177}Hf = 0.0384$), and t = the crystallization age of zircon.

4. Analytical results

The zircon U–Pb and Lu–Hf isotopic data are presented in Supplementary Tables A1 and A2, respectively, and are summarized in Table 1. Representative Cathoduluminescence (CL) images are given in Supplementary B, and some of them are shown in Fig. 2.

4.1. Zircon U–Pb isotopic results

The Gangdese zircons are mostly euhedral and reveal long to short prismatic forms, with average crystal lengths being ~150–300 μm and length-to-width ratios from 2:1 to 3:1 (Fig. 2, and Supplementary B).

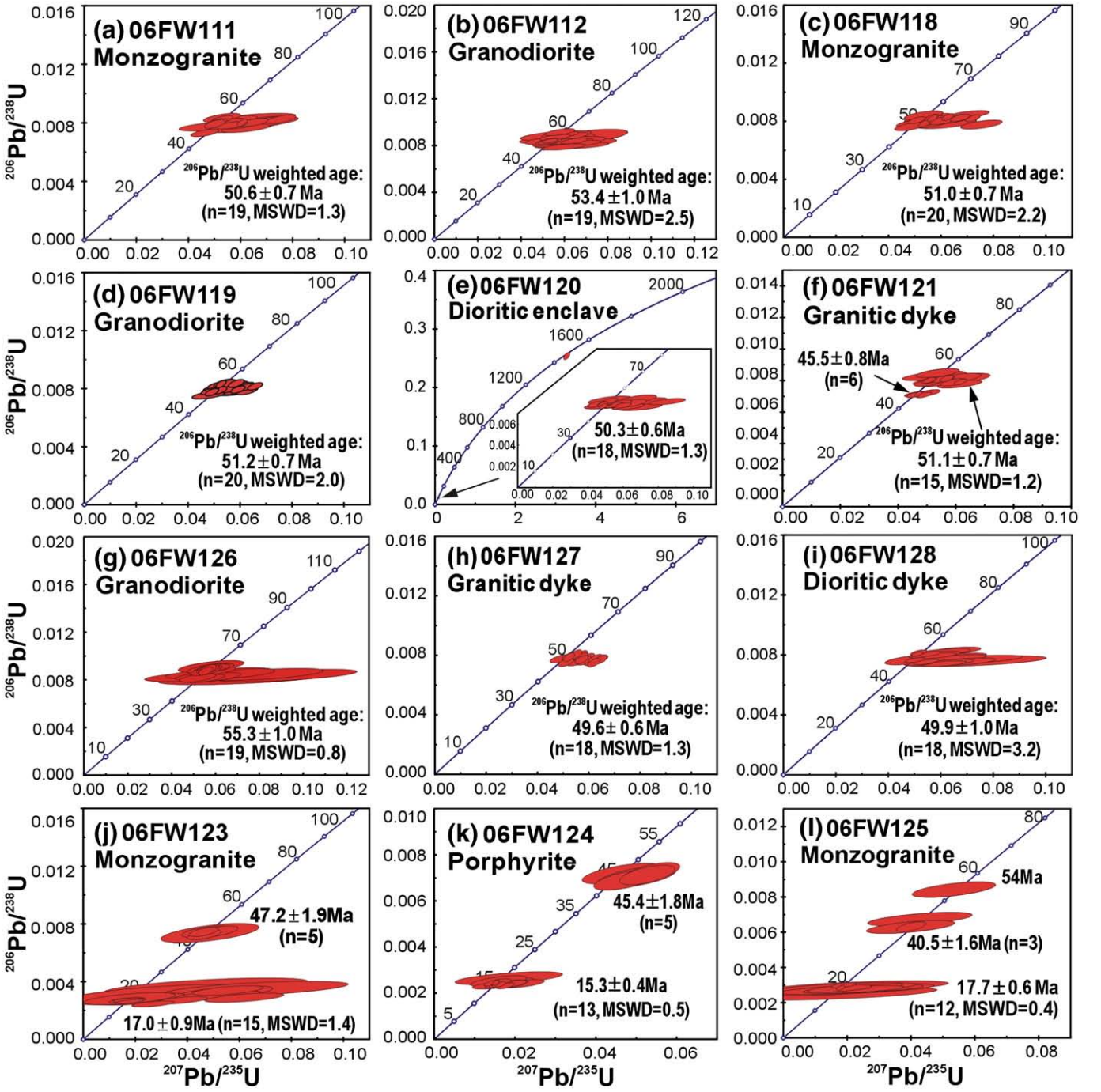

Fig. 5. U–Pb concordia diagrams of studied granites in the Quxu section (24 samples).

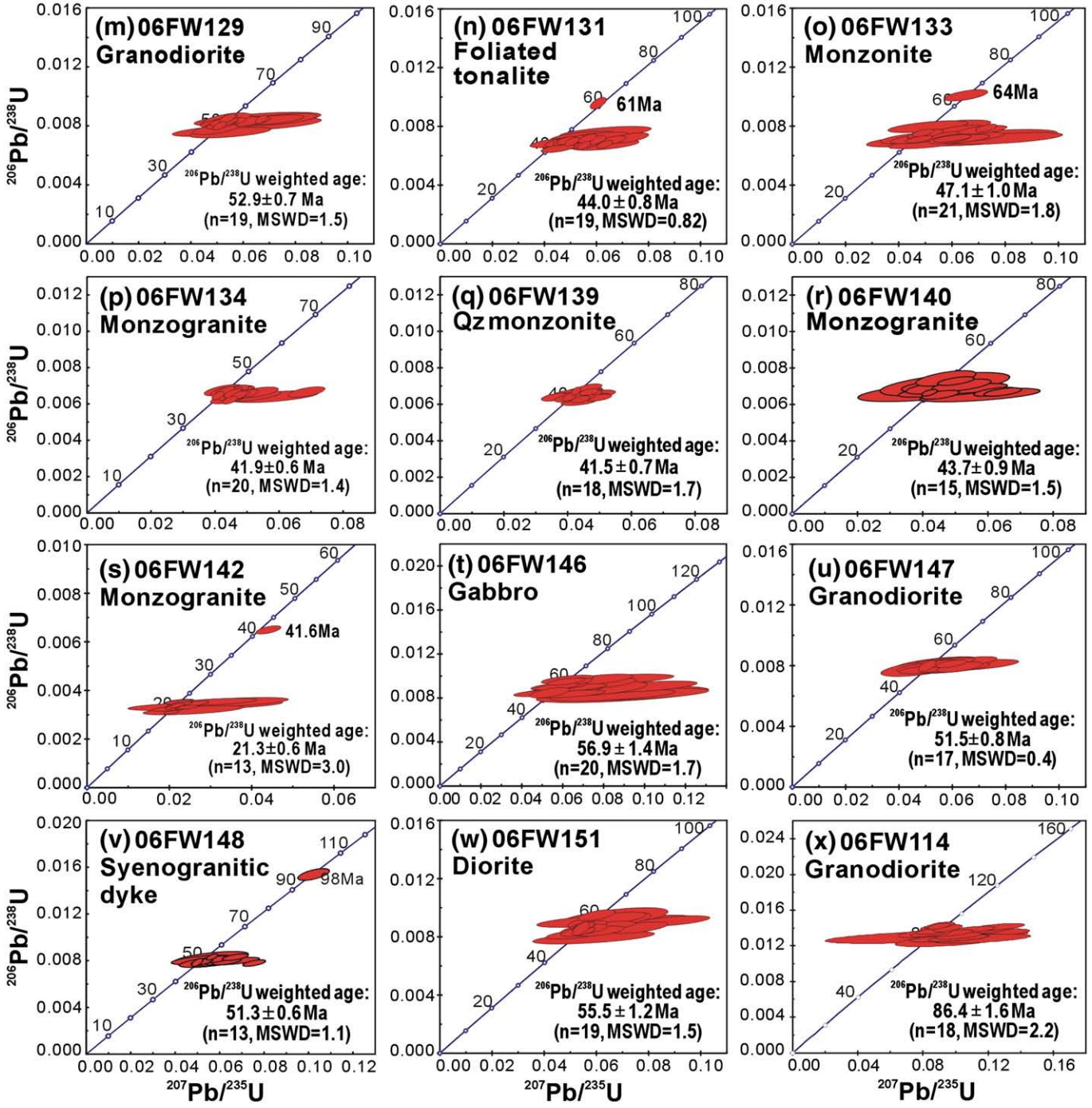

Fig. 5 (*continued*).

Most zircons are transparent, colorless to palely brown and show oscillatory zoning indicative of magmatic growth (Fig. 2, and Supplementary B). Thus, the interpretation of the zircon U–Pb isotopic results (see below) is simple and the obtained ages are interpreted as representing the crystallization timing of the zircons dated and thus the emplacement timing of the host rocks.

4.1.1. Lhasa–Gurong section

Five samples were dated from the granites exposed around Lhasa. Samples 06FW101 and 06FW104, from the Lhasa pluton, are both monzogranite. U–Pb isotopic analyses yielded identical zircon $^{206}Pb/^{238}U$ ages of 64.7 ± 1.1 and 64.4 ± 0.9 Ma, respectively (Fig. 3a and b). Samples 06FW105, 06FW108 and 06FW110 were collected from the Gurong pluton, which, ~30 km northwest of Lhasa, consists mainly of porphyritic granodiorite and monzogranite. The three samples yielded zircon $^{206}Pb/^{238}U$ ages of 55.2 ± 1.5, 56.8 ± 0.7 and 54.3 ± 0.9 Ma (Fig. 4a, b and c), slightly younger than those of the Lhasa pluton.

4.1.2. Quxu section

Granites around Quxu area show various rock types from gabbro, diorite, granodiorite and monzogranite (Schärer et al., 1984b; Dong et al., 2005; Mo et al., 2005b). Twenty-four samples were collected for zircon U–Pb dating in this study. Samples 06FW111 and 06FW112, being porphyritic monzogranite and coarse-grained granodiorite, respectively, from east of the Lhasa River, yielded zircon $^{206}Pb/^{238}U$ ages of 50.6 ± 0.7 and 53.4 ± 1.0 Ma (Fig. 5a and b). More specifically, the granites around

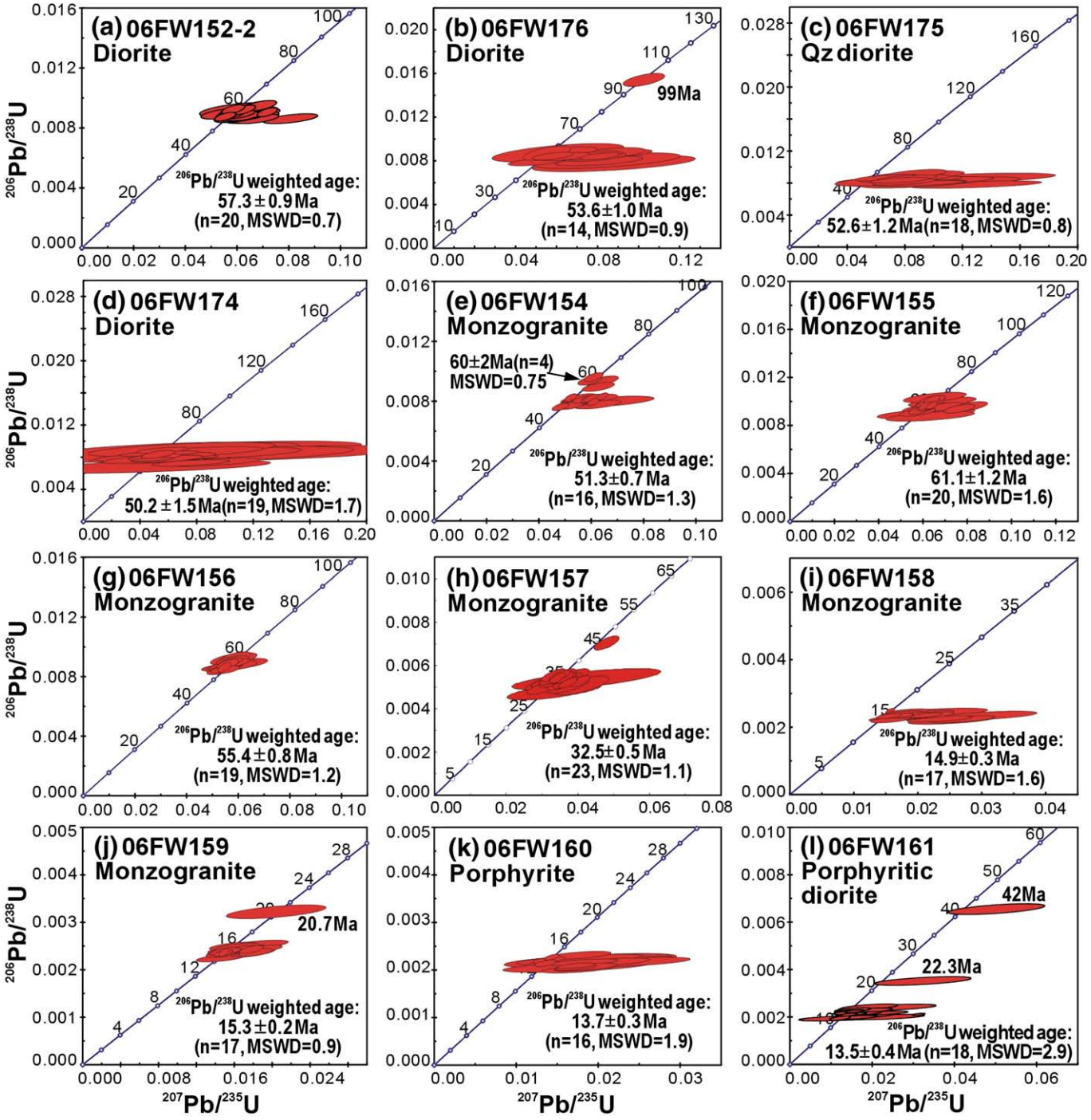

Fig. 6. U–Pb concordia diagrams of studied granites in the Nymo section (12 samples).

are characterized by the common occurrence of gabbroic–dioritic enclaves in granitic hosts. This study analyzed a medium- to coarse-grained monzogranite (06FW118) that changes gradually to granodiorite (06FW119) when dioritic enclave (06FW120) is abundant. U–Pb analyses give ^{206}Pb/^{238}U ages of 51.0 ± 0.7, 51.2 ± 0.7 and 50.3 ± 0.6 Ma, respectively (Fig. 5c–e), identical to the SHRIMP zircon U–Pb results of 51.2 ± 1.1 (granite), 47 ± 1.0 (gabbro) and 51.1 ± 1.1 Ma (enclave) from the same locality (Mo et al., 2005b). In addition, both granodiorites and enclaves in this locality are intruded by a later fine-grained monzogranitic vein (06FW121), in which most zircon grains give an age of 51.1 ± 0.7 Ma (Fig. 5f) and six zircon grains with high U contents and black CL images (see Fig. 2 and Supplementary B) give younger ages of 45.5 ± 0.8 Ma. The former could be interpreted as crystallization age of the zircons, whereas the later reflects the effect of metamictization which may lower the age of zircons. In another locality, coarse-grained granodiorite (06FW126) with a ^{206}Pb/^{238}U age of 55.3 ± 1.0 Ma (Fig. 5g) was cut by a composite felsic–mafic dyke (the mafic dyke outcrops within the felsic dyke along the strike), in which the felsic (06FW127) and mafic (06FW128) rocks give ^{206}Pb/^{238}U ages of 49.5 ± 0.6 and 49.9 ± 1.0 Ma, respectively (Fig. 5h and i). All these data support the conclusion obtained from field investigation that a significant magma mixing took place during the emplacement of granitic and mafic magmas at ~50 Ma.

In northern part of the Quxu section, there are fine-grained monzogranite (06FW123 and 06FW125) and porphyrite (06FW124)

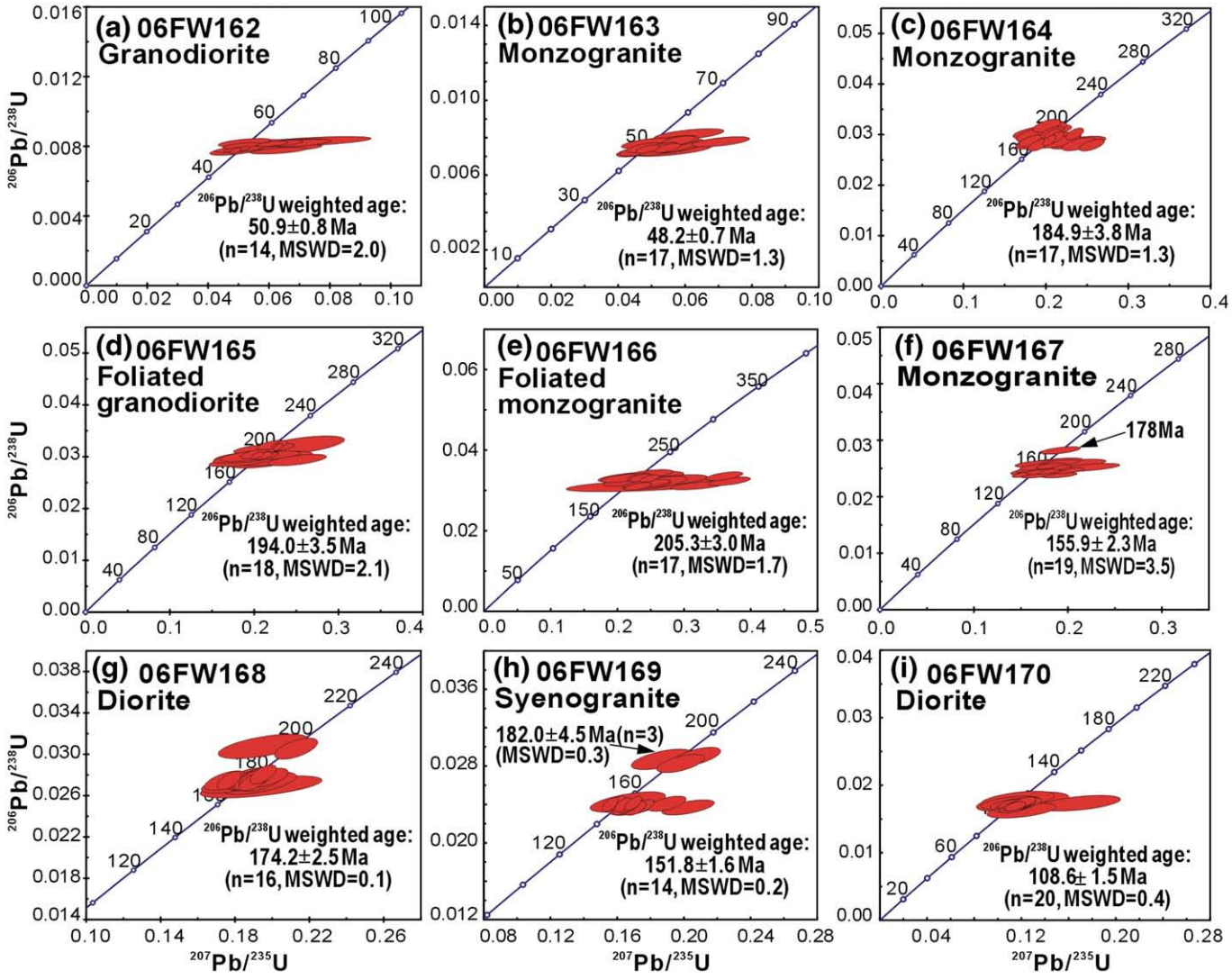

Fig. 7. U–Pb concordia diagrams of studied granites in the Dazhuqu section (9 samples).

near the Dabu copper deposit that show Miocene zircon $^{206}Pb/^{238}U$ ages ranging from 15.3 ± 0.4 to 17.7 ± 0.6 Ma (Fig. 5j–l). Five samples from southeast part of this pluton yielded zircon $^{206}Pb/^{238}U$ ages of 41.5 ± 0.7–52.9 ± 0.7 Ma (Fig. 5m–q), among which samples 06FW134 and 06FW139, from both sides of the Quxu bridge across the Lhasa River, show identical and young ages of 41.9 ± 0.6 and 41.5 ± 0.7 Ma, consistent with the conventional zircon U–Pb age of 41.7 ± 0.4 Ma reported by Schärer et al. (1984b). Moreover, in the field we observed the presence of amazonite-bearing pegmatite that occurs as veins cutting sample 06FW134, indicating a high degree of crystal fractionation in the evolution of this stage of granitic magmatism.

Seven samples from the western part of the Quxu section display diverse U–Pb age results. A coarse-grained monzogranites with weak foliation has a $^{206}Pb/^{238}U$ age of 43.7 ± 0.9 Ma (Fig. 5r), whereas an unfoliated monzogranite from nearby area show a $^{206}Pb/^{238}U$ age of 21.3 ± 0.6 (Fig. 5s). A monzodiorite collected from a norite–gabbro pluton north of Quxu gives a $^{206}Pb/^{238}U$ age of 56.9 ± 1.4 Ma (Fig. 5t), and the other three samples, ranging from diorite to syenogranite, show zircon ages from 51.3 ± 0.6 to 55.5 ± 1.2 Ma (Fig. 5u–w). However, sample 06FW114, a medium-grained granodiorite that has weak foliations and was collected from the northeastern most, yielded a Cretaceous $^{206}Pb/^{238}U$ age of 86.4 ± 1.6 Ma (Fig. 5x), much older than the Cenozoic zircon ages in all other samples.

4.1.3. Nymo section

The Nymo section is characterized by a large dioritic outcrop in its southern part (Fig. 1b). Four samples (06FW152-2, 06FW176, FW175 and 06FW174) collected from this diorite body yielded zircon $^{206}Pb/^{238}U$ ages of 57.3 ± 0.9 (Fig. 6a), 53.6 ± 1.0 (Fig. 6b), 52.6 ± 1.2 (Fig. 6c) and 50.2 ± 1.5 Ma (Fig. 6d), respectively, identical to those of dioritic rocks exposed in the Quxu pluton. Three samples (06FW154, 06FW155 and 06FW156) collected from the northeastern part are coarse-grained porphyritic monzogranite that give $^{206}Pb/^{238}U$ ages of 51.3 ± 0.7 (Fig. 6e), 61.1 ± 1.2 (Fig. 6f) and 55.4 ± 0.8 Ma (Fig. 6g), similar to the dioritic rocks. Unexpectedly, another porphyritic monozogranite (06FW157) collected from southeast of Nymo yielded Oligocene age of 32.5 ± 0.5 Ma (Fig. 6h). However, in western part of the Nymo pluton where the Chongjiang copper deposit is located, two porphyritic monzogranites (06FW158 and 06FW159) have Miocene zircon ages of 14.9 ± 0.3 (Fig. 6i) and 15.3 ± 0.2 Ma (Fig. 6j). Besides, a granitic porphyry (06FW160) and a porphyritic diorite (06FW161) give slightly younger ages of 13.7 ± 0.3 (Fig. 6k) and 13.5 ± 0.4 (Fig. 6l) than the hosted porphyritic monzogranite.

4.1.4. Dazhuqu section

Nine samples were collected from the Dazhuqu section along the roadcut north of the Dazhuqu township. Sample 06FW162 is a weakly

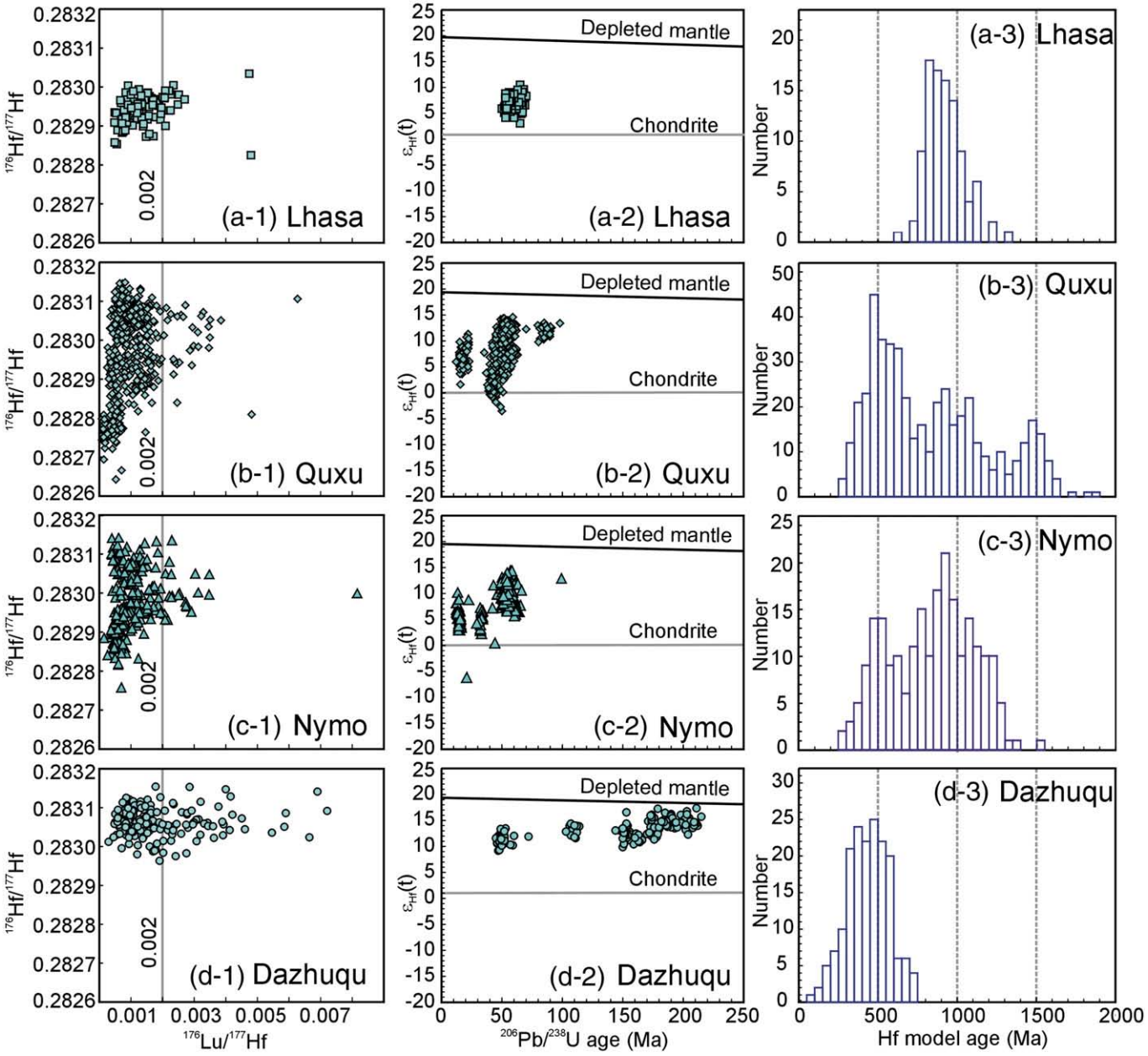

Fig. 8. Zircon Lu–Hf isotopic compositions of studied granites in the Gangdese batholith. All these zircons are characterized by high $^{176}Hf/^{177}Hf$ isotopic ratios, hence positive $\varepsilon_{Hf}(t)$ values and young Hf model ages. (a) $^{176}Lu/^{177}Hf$–$^{176}Hf/^{177}Hf$ variations; (b) $^{206}Pb/^{238}U$ age–$\varepsilon_{Hf}(t)$ variations; and (c) histograms of the two-stage Hf model ages.

foliated granodiorite from the northernmost and is cut by a monzogranite vein (sample 06FW163). Their zircon $^{206}Pb/^{238}U$ ages are 50.9 ± 0.8 (Fig. 7a) and 48.2 ± 0.7 (Fig. 7b), respectively. By contrast, other samples show totally different zircon ages. A fine-grained monzogranite has a $^{206}Pb/^{238}U$ age 184.9 ± 3.8 (Fig. 7c), which is identical to the $^{206}Pb/^{238}U$ age of 188.1 ± 1.4 Ma obtained by Chu et al. (2006) using SHRIMP technique. Further south of the above locality, two highly foliated samples, i.e., a granodiorite (06FW165) and a monzogranite (06FW166), yield $^{206}Pb/^{238}U$ ages of 194.0 ± 3.5 (Fig. 7d) and 205.3 ± 3.0 (Fig. 7e), respectively. The latter is the oldest zircon U–Pb age so far obtained for the granites within the Gangdese batholith. To further south, a monzogranite and a syenogranite give Jurassic zircon ages of 155.9 ± 2.3 (Fig. 7f) and 151.8 ± 1.6 (Fig. 7h) Ma, and a dioritic enclave gives a slightly older age of 174.2 ± 2.5 Ma (Fig. 7g). Near the Dazhuqu township, a diorite sample (06FW170) gives a Cretaceous $^{206}Pb/^{238}U$ age of 108.6 ± 1.5 Ma (Fig. 7i).

4.2. Zircon Lu–Hf isotopic results

In Table 1, the $\varepsilon_{Hf}(t)$ value, i.e., parts in 10^4 deviation of initial $^{176}Hf/^{177}Hf$ isotopic ratios between the sample and the chondritic uniform reservoir, and T_{DM2}, the two-stage zircon Hf isotope model age based on a depleted-mantle source and an assumption that the protolith of the zircon's host magma has the average continental crustal $^{176}Lu/^{177}Hf$ ratio of 0.015, were calculated after Griffin et al. (2002) by utilizing the ^{176}Lu–^{176}Hf decay constant adopted in Scherer et al. (2001). Our conclusions would not be significantly affected if the alternative decay constants proposed by other studies were used.

4.2.1. Lhasa–Gurong section

Zircons from this section are mostly low $^{176}Lu/^{177}Hf$ (<0.002) zircons with $^{176}Hf/^{177}Hf$ isotopic ratios ranging from 0.282825 to

0.283034 (Fig. 8a-1 and a-2). The calculated averages of $\varepsilon_{Hf}(t)$ values for the 5 Paleocene–Eocene samples range from 7.9 ± 0.3 to 6.0 ± 0.4, yielding two-stage Hf model ages of ~631–1305 Ma (Fig. 8a-3).

4.2.2. Quxu section

Zircons from this section show a large variation in Hf isotopic compositions, with $\varepsilon_{Hf}(t)$ values varying from 13.4 ± 0.3 to 0.6 ± 0.5 (Fig. 8b-1 and 4b-2), which result in a wide range of the Hf model ages (~253–1893 Ma; Fig. 8b-3). Different from the Lhasa–Gurong section, a few samples from this section show much lower $^{176}Lu/^{177}Hf$ (<0.0001) coupled with $^{176}Hf/^{177}Hf$ ratios (<0.282650), which will be discussed in the next section.

4.2.3. Nymo section

The zircon Hf isotopic ratios of this section are similar to those of the Lhasa–Gurong samples. The $^{176}Lu/^{177}Hf$ ratios are mostly less than 0.002 and the $^{176}Hf/^{177}Hf$ ratios range from 0.282846 to 0.283142 (Fig. 8c-1 and c-2). The calculated average $\varepsilon_{Hf}(t)$ values of the 12 samples range from 12.9 ± 0.4 to 4.6 ± 0.5. The Paleocene–Eocene samples ($n = 7$) have $\varepsilon_{Hf}(t)$ values of 12.9 ± 0.4 to 7.7 ± 0.7, slightly higher than those (6.4 ± 0.6 to 4.6 ± 0.5) of the Oligocene–Miocene samples ($n = 5$).

4.2.4. Dazhuqu section

Zircons from the Dazhuqu area show the highest $^{176}Lu/^{177}Hf$ and $^{176}Hf/^{177}Hf$ ratios (Fig. 8d-1 and d-2) among the four sections. The calculated averages of $\varepsilon_{Hf}(t)$ values range from 15.3 ± 0.4 to 11.0 ± 0.4, yielding the youngest two-stage Hf model ages of 92–746 Ma, indicating that the magma source of the granites in this area is relatively more juvenile than that of the other three sections.

5. Discussion

5.1. Geochronological framework of the Gangdese batholith

Since the early 1980s (Schärer et al., 1984b), the Gangdese batholith has been served as a focus of the geochronological and petrogenetic studies in Tibet (e.g., Maluski et al., 1982; Copeland et al., 1987, 1995; Richter et al., 1991; Chung et al., 2005; Wen et al., 2008). The pioneering data indicate that the granites were mostly emplaced during the Paleocene–Eocene with minor emplacement taking place during the Cretaceous (Schärer et al., 1984b; Dong et al., 2005; Mo et al., 2005b, 2007). However, recent isotopic studies indicate that Miocene and Jurassic granitic intrusions were also developed within this large and composite batholith (Chung et al., 2003; Hou et al., 2004; Chu et al., 2006; Zhang et al., 2007a). Even so, the age distribution of the entire batholith remains unclear due to the limitation of sampling. Recently, Wen et al. (2008) reported a more detailed geochronological study that, in combination with published age data, led these authors to conclude that the modern Gangdese outcrop consists of two main stages of plutonism during the Late Cretaceous and early Paleogene, with minor Jurassic granites in localities.

Together with the published zircon U–Pb age data ($n = 59$), this study ($n = 50$) results in a larger dataset ($n = 109$) that identifies four stages of granitic activities in the Gangdese batholith during 205–152, 109–80, 65–41 and 33–13 Ma, respectively (Fig. 9). The Triassic–Jurassic granites are mostly located in the Dazhuqu section, which was identified first by Chu et al. (2006). Additional Jurassic granites were later documented by Zhang et al. (2007a) in the Nymo section and by Yang et al. (2008b) to a locality east of Lhasa city. In this study, six out of the nine samples from the Dazhuqu section yielded ages of 205–152 Ma, indicating that the amount of the Triassic–Jurassic granites might be more abundant than previously thought (cf. Chung et al., 2005).

The Cretaceous granites were recognized first by Schärer et al. (1984b) in the Dazhuqu section, and recently reported by McDermid et al. (2002) and Wen et al. (2008) in other areas. There are only two samples in this study showing Cretaceous ages, i.e., 86.4 ± 1.6 Ma for sample 06FW114 and 108.6 ± 1.5 Ma for sample 06FW170. The former is a medium-grained granodiorite from the Quxu section, and the latter is a diorite from the northern Dazhuqu section. By contrast, ten out of 25 samples reported by Wen et al. (2008), which deals with a full areal coverage of the Gangdese batholith, show zircon U–Pb ages of 103–80 Ma. A direct inference is hence that Cretaceous granites were more extensively developed in other parts of the Gangdese batholith than its middle part investigated by this study.

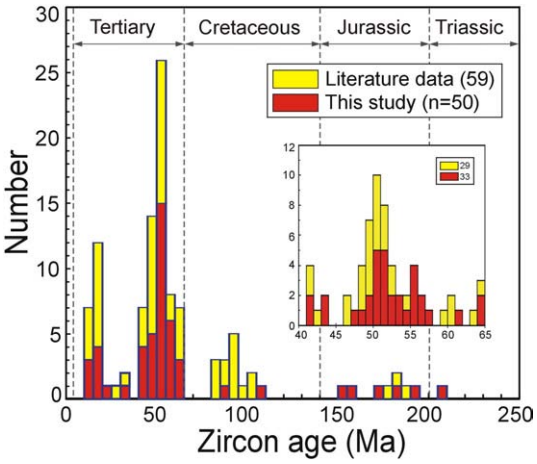

Fig. 9. Histogram of zircon U–Pb ages for granites in the Gangdese batholith. Four individual mgmatic stages can be recognized with the early Cenozoic (65–41 Ma) as the dominant. Literature data include Schärer et al. (1984b), Harrison et al. (2000), McDermid et al. (2002), Chung et al. (2003); Hou et al. (2004); Rui et al. (2003), Lin et al. (2004), Dong et al. (2005), Mo et al. (2005b), Chu et al. (2006), Mo et al., 2006; Wang et al. (2006), Zhang et al. (2007a), Wen et al. (2008) and Yang et al. (2008b). The inserted show the detailed age spectrum of the early Cenozoic granites in the Gangdese batholith.

The third and most prominent period of granitic magmatism for the Gangdese batholith is during the Paleocene–Eocene. Thirty-three out of 50 dated samples in this study have zircon U–Pb ages of 64–42 Ma. Among the 59 ages available from literature, 29 samples have zircon U–Pb ages of 65–41 Ma. Therefore, we conclude that the duration of 65–41 Ma is the most important period of the Gangdese magmatism. This granitic magmatism is also matched by coeval volcanism of the Linzizong successions (Mo et al., 2003, 2007, 2008; Zhou et al., 2004).

In addition, Miocene granites represent another important stage of magmatism in the Gangdese batholith. Chung et al. (2003) reported this stage of granites first from Linzhi and Jiama although a 30-Ma Oligocene granite had been previously reported by Harrison et al. (2000). Later study suggested that the copper deposits in the Gangdese batholith are mostly concentrated in this stage of granites (Hou et al., 2004). In the present study, samples from Nanmu (Dabu) and Chongjiang show zircon U–Pb ages of 13.5–17.7 Ma, with another sample (06FW142) from northwest of Quxu having zircon U–Pb age of 21 Ma. An unexpected age of 32.5 Ma obtained from 06FW157 in southeast of Nymo is coeval to the Yaja granodiorite (30.4 Ma) from Zedong area (Harrison et al., 2000). It should be noted that the Miocene granites show the same geological and petrological characteristics as those of the Paleocene–Eocene granites, which means that more field investigation is needed to distinguish the different stages of granites in this batholith since almost all these granites were classified as being Paleocene–Eocene in the previous geological maps.

The identification of above four stages of granitic magmatism for the Gangdese batholith is also supported by radiometric dating of associated volcanic rocks. Along with the Miocene and Paleocene–Eocene (Linzizong) volcanic rocks (Coulon et al., 1986; Turner et al., 1993, 1996; Williams et al., 2001, 2004; Zhou et al., 2004; He et al.,

2007; Lee et al., 2007; Mo et al., 2003, 2007, 2008), recent mapping projects involving detailed field investigations indicated that Jurassic (182–174 Ma) and Cretaceous (120–110 Ma) volcanic rocks are widespread within the Gangdese batholith (Dong et al., 2006; Geng et al., 2006; Zhu et al., 2008). Additionally, U–Pb isotopic dating for the detrital zircons from the Cretaceous Xigaze fore-arc basins, which accumulated the eroded sediments from the Gangdese arc (Einsele et al., 1994; Dűrr, 1996), revealed that the Gangdese batholith was dominated by igneous rocks formed at ca. 130–80 Ma, associated with smaller amounts formed at ca. 190–150 Ma, recording two important stages of the arc magmatism during the Mesozoic (Wu et al., 2009).

5.2. Hf isotopes and juvenile nature of the Gangdese batholith

The Lu–Hf isotope, as many other isotopic systems, is an important geochemical tracer to decipher the evolutionary history of the crust and mantle. During partial melting, the once uniform mantle would generate Lu/Hf fractionation with formation of basaltic magma (low Lu/Hf) and mantle residue (high Lu/Hf) (Kinny and Maas, 2003). Consequently, the residual and depleted mantle, which has Lu/Hf > chondrites, will be progressively radiogenic with positive ε_{Hf} value. In contrast, the enriched, especially the ancient crust, with Lu/Hf < chondrites, will be unradiogenic with negative ε_{Hf} value. If the magma derives from the juvenile crust, it still has positive ε_{Hf} value since there is no enough time for it to deviate from the mantle value. However, mixing between the depleted and enriched source derived magmas will have variable ε_{Hf} values depending on the mixing proportions.

Zircon is a common accessory mineral in granites. Its high concentration of Hf element, usually 0.5–2%, makes precise measurement of Hf isotopic ratios ($^{176}Hf/^{177}Hf$) feasible using laser ablation technique. Moreover, the extremely low Lu concentration relative to Hf means that the $^{176}Hf/^{177}Hf$ ratio of zircon can represent the initial Hf isotopic composition of the magma from which the zircon crystallized because subsequent radiogenic growth is negligible (Kinny and Maas, 2003). Combined with its high resistance to weathering and/or alteration, zircon Hf isotope has been proven as an excellent geochemical tracer to decipher magma source and petrogenetic processes (Kemp et al., 2006; Yang et al., 2007). Considering that the granites are mostly crustal derived, the positive and negative ε_{Hf} values of their zircons would indicate that they come from partial melting of juvenile and ancient crusts, respectively (Kinny and Maas, 2003).

According to published data (Chu et al., 2006; Zhang et al., 2007a), the Jurassic granites in the Gangdese batholith is characterized by high and positive $\varepsilon_{Hf}(t)$ values. As for younger granites of the other three stages, no Hf isotopic data has been reported although it was quoted that they show the same positive $\varepsilon_{Hf}(t)$ values (Chu et al., 2006; Liang et al., 2008). In this study, Hf isotopic ratios have been measured simultaneously with the U–Pb ages. As shown in Fig. 8, all granites from the Gangdese batholith display positive zircon $\varepsilon_{Hf}(t)$ values. It has been generally suggested that granites in the world are mostly derived from partial melting of pre-existed crust, manifest by their negative $\varepsilon_{Nd}(t)$ or $\varepsilon_{Hf}(t)$ values (Allègre and Ben Othman, 1980). However, Hf isotopic compositions of granites from the Gangdese batholith reflect a remarkable difference from most granites worldwide and the positive $\varepsilon_{Hf}(t)$ values indicate a very juvenile magma source of this batholith.

Across the southern margin of the Lhasa terrane, the Transhimalayan batholith can be divided into the Kohistan–Ladakh batholith in the west, the Gangdese batholith in the middle and the Chayu–Dianxi–Burma batholith in the east (Allègre et al., 1984; Le Fort, 1988; Barley et al., 2003) (Fig. 1a). As discussed above, the Gangdese batholith is characterized by four distinct stages of granitic magmatism showing positive $\varepsilon_{Hf}(t)$ values (Fig. 10). Zircon U–Pb age dating of granites in the Kohistan–Ladakh batholith indicated that this composite batholith was also mostly emplaced during 103–50 Ma, with a magmatic gap around 80–70 Ma (Honegger et al., 1982;

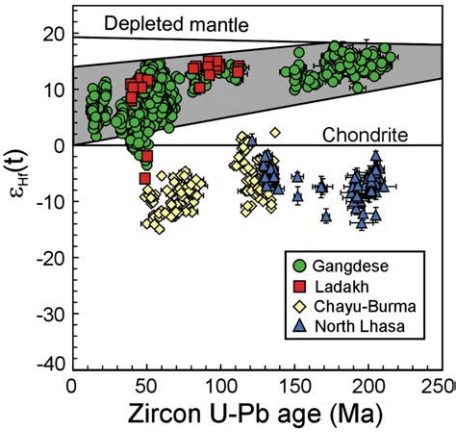

Fig. 10. Comparisons of zircon Hf isotopic compositions from different batholiths in the Transhimalayan belt and the northern Lhasa terrane. It is indicated that zircons from the Gangdese and Ladakh batholiths show characterized positive $\varepsilon_{Hf}(t)$ values, whereas those from the Chayu–Burma batholith and the North Lhasa terrane show negative $\varepsilon_{Hf}(t)$ values; suggesting that they derived from the juvenile and ancient crusts, respectively. Data source: Gangdese batholith: Chu et al. (2006), Zhang et al. (2007a) and this study; Ladakh: Schaltegger et al. (2002) and Heuberger et al. (2007); Dianxi–Burma: Liang et al. (2008); Northern Lhasa: Chu et al. (2006), Zhang et al. (2007a) and unpublished data of authors. The grey shaded area represents the Hf isotopic evolutional trend of the analyzed zircons.

Schärer et al., 1984a; Weinberg and Dunlap, 2000; Pedersen et al., 2001; Dunlap and Wysoczanski, 2002; Schaltegger et al., 2002; Jain and Singh, 2008). This batholith show also positive zircon $\varepsilon_{Hf}(t)$ values between +6 and +15 (Schaltegger et al., 2002; Heuberger et al., 2007; Ravikant et al., in press, Fig. 10). To the east, however, the Chayu–Dianxi–Burma batholith is characterized by negative $\varepsilon_{Hf}(t)$ values (Liang et al., 2008; Chiu et al., 2009) (Fig. 10). In this regard, the geochronological framework and positive $\varepsilon_{Hf}(t)$ values of the Kohistan–Ladakh–Gangdese batholith have broad implications to decipher the erosion history of the Himalaya–Tibet orogen, since according to our knowledge, there is no other area in the Himalaya–Tibet region from which rocks show the similar geochronological and isotopic features. For example, zircons from the granites in the Himalaya and northern Lhasa terrane show only negative $\varepsilon_{Hf}(t)$ values (Chu et al., 2006; Zhang et al., 2007b) (Fig. 10), markedly different from those of the Kohistan–Ladakh–Gangdese batholith. Therefore, the unique zircon Hf isotopic compositions, marked with high, positive $\varepsilon_{Hf}(t)$ values, observed in the Kohistan–Ladakh–Gangdese granites can be used as an effective geochemical tracer to study the source-to-sink relationship of the sediments eroded from the southern Tibetan Plateau (Wu et al., 2007, 2009; Liang et al., 2008).

5.3. Petrogenesis and geodynamic implications

Before discussing the petrogenesis of the studied granites and their geodynamic implications, it is necessary to make clear the collision time between India and Asia since this issue is quiet debatable recently. According to the available literature, the proposed initial time of India–Asia collision varies from ~70 to 34 Ma (Najman, 2006, and references therein), including constraints from paleomagnetism (Patriat and Achache, 1984; Besse and Courtillot, 1988; Klootwijk et al., 1992; Patzelt et al., 1996; Aitchison et al., 2007), floral to faunal distribution (Jaeger et al., 1989; Prasad et al., 1994; Upadhyay et al., 2004), cessation of marine facies and change of sedimentation patterns (Garzanti et al., 1987, 1996; Willems et al., 1996; Searle et al., 1997; Rowley, 1998; Zhu et al., 2005), development of flexure-related unconformities in the suture zone and both continental margin (Beck et al., 1995; Yin and Harrison, 2000; Ding et al., 2005; Mo et al., 2007, 2008), metamorphic time of eclogites by continental subduction (Tonarini et al., 1993; de Sigoyer et al., 2000; Kaneko et al., 2003;

Leech et al., 2005) and the end of Gangdese I-type granitoid injection (Searle et al., 1987). Considering a large pile of data and discussion, only a brief introduction about the collisional time in Tibet is concerned here.

Based on the paleomagnetic data for the Cretaceous–Paleocene rocks on both sides of the Yarlung-Tsangpo, it was proposed that the initial contact between India and Asia might take place at ~65–60 Ma with complete suturing at ~55–50 Ma in Tibet (Patzelt et al., 1996). In terms of variations of sedimentation facies and depositional patterns of the Cretaceous–Paleocene rocks in Tibet, Willems et al. (1996) proposed that the collision initiated at ~70–64 Ma. However, this conclusion was challenged by Rowley (1996, 1998) who suggested that collision occurred after 46 Ma. Recently, Zhu et al. (2005) suggested that the onset of the India–Asia collision occurred at 50.6 ± 0.2 Ma based on source changes of the sedimentary rocks in southern Tibet. With respect to the deformation, Ding et al (2005) advocated that the obduction of the oceanic rocks onto the northern margin of the India at ~65 Ma marks the India–Asia collision at that time. This conclusion is also supported by Mo et al. (2005a, 2007) who suggested that the unconformity between the Linzizong volcanic sequence and the underlying Cretaceous rocks at ~65 Ma represents the India–Asia collision.

Although it seems widely accepted that the initial collision between India and Asia took place before 50 Ma, even older than 70 Ma, Aitchison et al. (2000, 2007) proposed that the above collision did not take place until ~34 Ma. They suggested that an intraoceanic arc (Zedong terrane) collided with India firstly at ~55 Ma, and then the composite Indian continent eventually collided with Asia at ~34 Ma when the marine environment ended. It is beyond this paper to review all lines of evidence they based on, our argument is that the Zedong terrane might be the slice of the Gangdese batholith (Chung, unpublished data), let alone the small size of the Zedong terrane compared with the huge Neo-Tethysan ocean. Therefore, we suggest that the previous conclusion based on multidisciplinary lines of direct and indirect evidence is solid as proposed by comment of Garzanti (2008). It is still unclear, however, that the collision took place at ~70–65 or ~55 Ma. We will discuss this issue below based on our new age data since it is the key for us to give a reasonable explanation for the petrogenesis of the Gangdese batholith.

Previously, it was thought that the Gangdese batholith was formed by partial melting of mantle wedge above subduction zone of the Neotethyan ocean beneath the southern Asian continent (Searle et al., 1987; Rowley, 1996), or resulted from India–Asian collision (Debon et al., 1986). The identification of multiple stages of granites challenges these interpretations. Before dealing with the petrogenesis of these stages of magmatism, however, we firstly discuss the source characteristics of these granitic rocks. As stated above, no significant Hf isotopic difference has been documented between the mantle-derived gabbro and diorite and crustal-derived granites (including granodiorite, monzogranite and syenogranite), which means that either the crustal- and mantle-derived magmas had become isotopically homogeneous during magma mixing, or they share a common isotopic source. Taking an example of a suite of samples 06FW118, 06FW119, 06FW120 and 06FW121 from the Quxu section, all of which were emplaced synchronically at ~51 Ma but represent product of different degree of magma mixing. The zircons from the above samples show different internal structures. Zircons from 06FW118 (monzogranite) and 06FW119 (granodiorite) show typical oscillatory growth zoning with fine bands (Fig. 2), and the zircons from sample 06FW120 display simple growth zone with broad bands (Fig. 2). In the later dyke of 06FW121, the zircons are mostly small with fine growth zoning (Fig. 2). All of these indicate that these zircons crystallized from different kinds of host magmas. Considering that zircon is generally crystallized during early evolution of granitic magma and records the initial Hf isotopic compositions of magma, we therefore propose that the crustal and mantle sources of the Gangdese granites are similar isotopically. This conclusion is supported by the temporal Hf isotopic variations in the granites, which follow an evolutional trend intersecting the depleted mantle at ~200–300 Ma (Fig. 10). Therefore, it is reasonable to conclude that all these granites, including associated gabbro and diorite, have a common source despite the overall magma evolution might be complex.

Both the subducted Neotethyan oceanic lithosphere and its resultant young mantle wedge can be the possible candidates of this common source and discrimination of these possibilities is not easy at this point. Generally, partial melting of subducted oceanic crust would result in formation of adakite (Defant and Drummond, 1990), which, however, is not identified for most of the Gangdese granites. Most recently, Yang et al. (2008a) reported the existence of eclogites with oceanic crustal affinity at Songduo, east of Lhasa (Fig. 1b), which led the authors to divide the Lhasa terrane into southern and northern portions. SHRIMP U–Pb dating of zircons from the eclogites yield a metamorphic age of 262 ± 5 Ma (Yang et al., 2008a). In addition, Late Permian arc-related granites and volcanic rocks were reported north of that boundary (Booth et al., 2004; Yang et al. 2008a). Given that the southern Lhasa terrane, occupied by the Gangdese batholith and associated volcanic rocks, extends in the west–east direction with a length of >1000 km and a width of ~100 km (Fig. 1a), we, therefore, propose an oceanic arc terrane that has positive $\varepsilon_{Hf}(t)$ values was

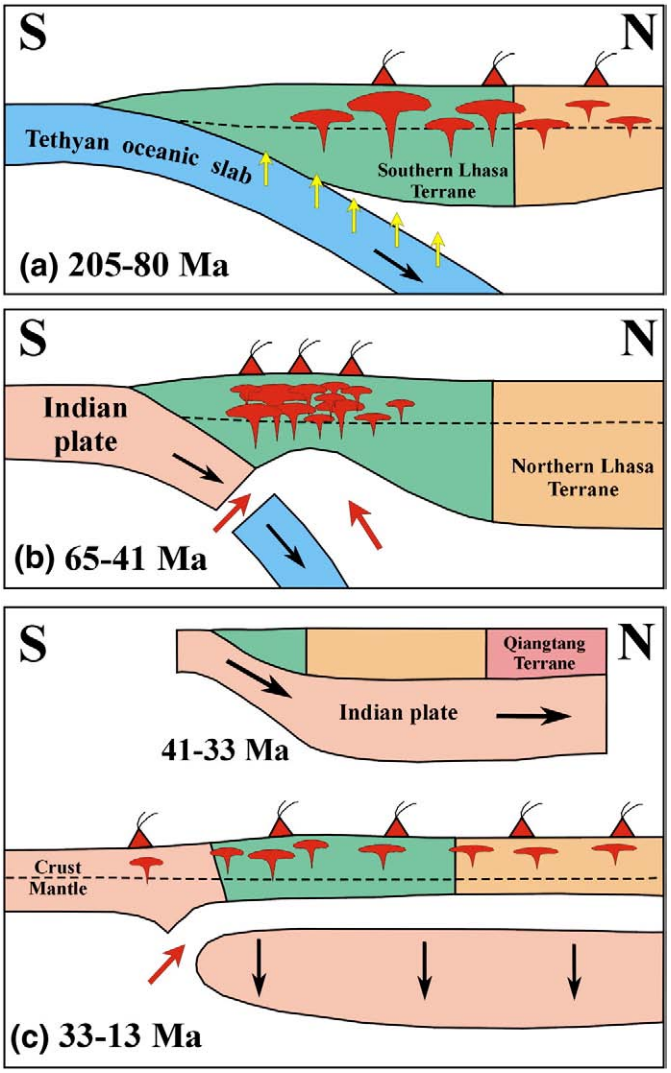

Fig. 11. Stages of Tibetan plateau evolution constrained from granites. (a) ~205–80 Ma: subduction of Neotethyan ocean beneath Lhasa terrane; and (b) ~65–41 Ma: the magmatic flare-up in southern Lhasa terrane (Gangdese batholith and Linzizong volcanic rocks); (c) ~33–13 Ma: Convective removal of the thickened Himalaya–Tibet mantle lithosphere. See text for details.

accreted to the southern Asian continental margin during the late Permian. This terrane then served as the magmatic source of the igneous rocks in the Gangdese batholith.

Although it was generally thought that the Neotethyan subduction started during the Cretaceous (Honegger et al., 1982; Schärer et al., 1984b), or middle Jurassic (Searle et al., 1999, 2007; Barley et al., 2003), Chu et al. (2006) argued that the subduction has begun since the early Jurassic. Our identification of granites aged 205–185 Ma in the Dazhuqu section raises the possibility of an even earlier start of the Neotethyan subduction. These rocks are foliated hornblende-bearing granodiorite–monzogranite, similar to the "typical" rock association formed in the convergent margin. The presence of Triassic–Jurassic granites in the northern Lhasa terrane (Li et al., 2003; He et al., 2005, 2006) led some authors to propose that there was a southward subduction of the Bangong ocean slab responsible for the petrogenesis of those granites (Geng et al., 2006; Pan et al., 2006). However, the Late Triassic–Jurassic granites we identified in Dazhuqu area locate very close to the Yarlung–Tsangpo suture. This, together with other Jurassic granites in the Gangdese batholith (Chu et al., 2006; Zhang et al., 2007b; Yang et al., 2008b), allow us to signify the importance of the northward Neotethyan subduction that began in the Late Triassic, at least since ~205 Ma, and lasted until the Late Cretaceous thus resulting in the Gangdese granites of 109–80 Ma (Fig. 11a).

The Gangdese magmatism is marked with a peak activity in the Paleocene–Eocene (65–41 Ma) (Fig. 9), forming a variety of rocks including gabbro, diorite, granodiorite, monzogranites and minor syenogranite. Petrological similarities between these rocks and those formed in the convergent settings led some authors to attribute their petrogenesis to the continued Neotethyan subduction (e.g., Schärer et al., 1984b). Other researchers, however, proposed that these rocks were formed in a syn-collisional setting related to the India–Asia collision starting ~70–65 Ma (Ding et al., 2005; Mo et al., 2007, 2008). Besides, it was suggested that the magmatism was initiated by rollback of the subducting Neotethyan oceanic slab and then culminated by the slab break-off that occurred around 50–45 Ma (Chung et al., 2005; Lee et al., 2007; Wen et al., 2008). Despite it is not easy to constrain the exact geodynamic settings solely by igneous records, the following lines of evidence lends supports to a model of rollback followed by slab break-off (Fig. 11b). Firstly, Based on the new $^{40}Ar/^{39}Ar$ age results for the volcanic rocks recovered from a large area in Tibet (29°N to 32°N and 85°E to 93°E), together with available literature data, Lee et al. (2009) delineated two discrete stages of volcanism, namely, a widespread Cretaceous stage and an intense, but spatially confined, Paleogene stage. The latter, occurring only in the southern part of the Lhasa terrane, resulted in the Linzizong volcanic successions (aged between ca. 65 and 41 Ma). Lee et al. (2009), furthermore, identify southward migration and intensification of the volcanism in the Lhasa terrane with magmatic "flare-up" at ca. 50 Ma. While the volcanic successions consist dominantly of calc-alkaline rocks typical of arc lava geochemistry, those formed during the flare-up period show significant compositional variations from low-K tholeiitic through calc-alkaline to shoshonitic magma suites. These observations led the authors to interpret the volcanic southward migration and following flare-ups as the consequences of rollback (65–50 Ma) and break-off (stated ~50 Ma) of the subducted Neotethyan slab that occurred ahead and in the early stage, respectively, of the India–Asia collision. Secondly, although it seems that there is no magmatic gap during 65–41 Ma (Fig. 9), the age statistics from granites show a flare-up around 50 Ma, implying that these rocks might not be formed in a single geological setting. Thirdly, overall speaking, the Paleocene–Eocene granites, especially those formed during 50–41 Ma, show more heterogeneous and lower $\varepsilon_{Hf}(t)$ values (Fig. 10), with some (samples of 06FW131, 06FW133 and 06FW139) showing negative $\varepsilon_{Hf}(t)$ values, than other stages of granites. Among them, the oldest granites showing low to negative $\varepsilon_{Hf}(t)$ values is 06FW133 which has a weighted $^{206}Pb/^{238}U$ age of 47.1 ± 1.0 Ma (Table 1). In sample 06FW133, two individual spots (04 and 05) yield $^{206}Pb/^{238}U$ ages of 50 ± 1 and 49 ± 2 Ma with $\varepsilon_{Hf}(t)$ values of −3.50 ± 0.92 and −2.70 ± 0.88. This phenomena was also observed in zircons from the Ladakh batholith in the west (Wu et al., 2007; Heuberger et al., 2007). Here we ascribe this feature of decreasing of $\varepsilon_{Hf}(t)$ values to the involvement of old crustal material, e.g., the Indian continental crust, which leads us to further infer the collision between India and Asia to have started before 50 Ma. Obviously, the geodynamic significance of the 65–41 Ma granites needs more work since this issue is closely related to the collisional time between India and Asia.

As for the Miocene granites, numerous studies have indicated that they are geochemically distinct from the granites of previous stages (Turner et al., 1993, 1996; Williams et al., 2001, 2004; Chung et al., 2003; Ding et al., 2003; Hou et al., 2004; Guo et al., 2007). These rocks are so called "collision-related" adakites, which resulted most likely from partial melting of a thickened mafic crust postdating the onset of the India–Asia collision (Chung et al., 2003, 2005; Guo et al., 2007). There are several possible mechanisms proposed for this stage of magmatism, i.e., break-off of the Neotethyan slab (Kohn and Parkinson, 2002), delamination or convective removal of the thickened lithospheric (Miller et al., 1999; Williams et al., 2001; Chung et al., 2003, 2005). Considering that this Oligocene–Miocene magmatism is at least 20–30 Ma later than the India–Asia collision as discussed above, the slab-breakoff model is not favored in this study. In contrast, lithospheric delamination or convective removal was proposed to interpreter the widespread occurrence of this post-collisional magmatism although distinguishing the two models is difficult (Fig. 11c).

In summary, Mesozoic granites in the Gangdese batholith were formed by the Neotethyan subduction but Cenozoic granites were formed in different geodynamic settings, i.e., the Paleocene–Eocene ones related to the slab break-off (Chung et al., 2005; Lee et al., 2007; Wen et al., 2008) and the Miocene ones to convective removal of the thickened lithosphere (Williams et al., 2001; Chung et al., 2003, 2005). Thus, the Gangdese magmatic evolution is more complicated than previously thought.

6. Conclusions

A comprehensive zircon U–Pb and Hf isotopic study of granites in the Gangdese batholith leads to the following conclusions:

1) The granites in the Gangdese batholith developed in four discrete stages, during 205–152, 109–80, 65–41 and 33–13 Ma, respectively, with the period of 65–41 Ma being the most prominent stage of the granitic magmatism.
2) The Gangdese batholith is characterized by positive $\varepsilon_{Hf}(t)$ values, yielding young Hf model ages, which suggests their derivation from juvenile crust and hence continental crustal growth during the Phanerozoic in this region.
3) Triassic-Cretaceous granites in the Gangdese batholith were formed by northward Neotethyan subduction beneath the Lhasa terrane, but the Paleocene-Eocene granites are unrelated to subduction and were probably triggered by slab break-off. The Miocene granites likely resulted from convective removal of lithosphere.
4) This study establishes a Gangdese zircon U–Pb and Hf isotope dataset that may serve as geochronological and isotopic fingerprints to effectively trace the erosion–deposition history around the Tibetan Plateau.

Acknowledgements

We thank Feng-Cai Luo for assistance with sample collection, Jin-Feng Sun and Yue-Heng Yang for help with LA-ICPMS analyses. Peter Clift and Yaoling Niu are thanked for their thoughtful reviews, which

greatly helped us to improve the paper. This study was financially supported by funds from the Chinese Academy of Sciences (KZCX2-YW-Q09-06) and the National Natural Science Foundation of China (Grant 40721062).

Appendix A. Supplementary data

Supplementary data associated with this article can be found, in the online version, at doi:10.1016/j.chemgeo.2009.01.020.

References

Aitchison, J.C., Badengzhu, Davis, A.M., Liu, J., Luo, H., Malpas, J., McDermid, I., Wu, H., Ziabrev, S., Zhou, M.F., 2000. Remnants of a Cretaceous intra-oceanic subduction system within the Yarlung–Zangbo suture (southern Tibet). Earth Planet. Sci. Lett. 183, 231–244.

Aitchison, J.C., Ali, J.R., Davis, A.M., 2007. When and where did India and Asia collide? J. Geophys. Res. 112, B05423. doi:10.1029/2006JB004706.

Allègre, C.J., Ben Othman, D., 1980. Nd–Sr isotopic relationship in granitoid rocks and continental crust development: a chemical approach to orogenesis. Nature 286, 335–342.

Allègre, C.J., Courtillot, V., Tapponnier, P., Hirn, A., Mattauer, M., Coulon, C., Jaeger, J.J., Achache, J., Schärer, U., Marcoux, J., Burg, J.P., Girardeau, J., Armijo, R., Gariépy, C., Göpel, C., Li, T.D., Xiao, X.C., Chang, C.F., Li, G.Q., Lin, B.Y., Teng, J.W., Wang, N.W., Chen, G.M., Han, T.L., Wang, X.B., Deng, W.M., Sheng, H.B., Cao, Y.G., Zhou, J., Qiu, H.R., Bao, P.S., Wang, S.C., Wang, B.X., Zhou, Y.X., Xu, R.H., 1984. Structure and evolution of the Himalaya–Tibet orogenic belt. Nature 307, 17–22.

Amelin, Y., Lee, D.C., Halliday, A.N., Pidgeon, R.T., 1999. Nature of the Earth's earliest crust from hafnium isotopes in single detrital zircons. Nature 399, 252–255.

Anderson, T., 2002. Correction of common lead in U–Pb analyses that do not report ^{204}Pb. Chem. Geol. 192, 59–79.

Barley, M.E., Pickard, A.L., Zaw, K., Rak, P., Doyle, M.G., 2003. Jurassic to Miocene magmatism and metamorphism in the Mogok metamorphic belt and the India–Eurasia collision in Myanmar. Tectonics 22. doi:10.1029/2002TC001398.

Beck, R.A., Burbank, D.W., Sercombe, W.J., Riley, G.W., Barndt, J.K., Berry, J.R., Afzat, J., Khan, A.M., Jurgen, H., Metje, J., Cheema, A., Shafique, N.A., Lawrence, R.D., Khan, M.A., 1995. Stratigraphic evidence for an early collision between northwest India and Asia. Nature 373, 55–58.

Besse, J., Courtillot, V., 1988. Paleogeographic maps of the continents bordering the Indian Ocean since the Early Jurassic. J. Geophys. Res. 93, 11,791–11,808.

Black, L.P., Kamo, S.L., Allen, C.M., Aleinikoff, J.N., Davis, D.W., Korsch, R.J., Foudoulis, C., 2003. TEMORA 1: a new zircon standard for Phanerozoic U–Pb geochronology. Chem. Geol. 200, 155–170.

Blichert-Toft, J., Albarede, F., 1997. The Lu–Hf isotope geochemistry of chondrites and the evolution of the mantle–crust system. Earth Planet. Sci. Lett. 148, 243–258.

Booth, A.L., Zeitler, P.K., Kidd, W.S.F., Wooden, J., Liu, Y.P., Idleman, B., Hern, M., Chamberlain, C.G., 2004. U–Pb zircon constrains on the tectonic evolution of southern Tibet, Namche Barwa area. Am. J. Sci. 304, 889–929.

Chiu, H.Y., Chung, S.L., Wu, F.Y., Liu, D.Y., Liang, Y.H., Lin, I.J., Iizuka, Y., Xie, L.W., Wang, Y.B., Chu, M.F., 2009. Zircon U–Pb and Hf isotopic constraints from eastern Transhimalayan batholiths on the precollisional magmatic and tectonic evolution in southern Tibet. Tectonophysics, in review.

Chu, M.F., Chung, S.L., Song, B., Liu, D.Y., O'Reilly, S.Y., Pearson, N.J., Ji, J.Q., Wen, D.J., 2006. Zircon U–Pb and Hf isotope constraints on the Mesozoic tectonics and crustal evolution of Southern Tibet. Geology 34, 745–748.

Chung, S.L., Liu, D.Y., Ji, J.Q., Chu, M.F., Lee, H.Y., Wen, D.J., Lo, C.H., Lee, T.Y., Qian, Q., Zhang, Q., 2003. Adakites from continental collision zones: melting of thickened lower crust beneath southern Tibet. Geology 31, 1021–1024.

Chung, S.L., Chu, M.F., Zhang, Y.Q., Xie, Y.W., Lo, C.H., Lee, T.Y., Lan, C.Y., Li, X.H., Zhang, Q., Wang, Y.Z., 2005. Tibetan tectonic evolution inferred from spatial and temporal variations in post-collisional magmatism. Earth Sci. Rev. 68, 173–196.

Copeland, P., Harrison, T.M., Kidd, W.S.F., Xu, R., Zhang, Y., 1987. Rapid early Miocene acceleration of uplift in the Gangdese Belt, Xizang (southern Tibet), and its bearing on accommodation mechanisms of the India–Asia collision. Earth Planet. Sci. Lett. 86, 240–252.

Copeland, P., Harrison, T.M., Yun, P., Kidd, W.S.F., Royden, M., Zhang, Y., 1995. Thermal evolution of the Gangdese batholith, southern Tibet: a history of episodic unroofing. Tectonics 14, 223–236.

Coulon, C., Maluski, H., Bollinger, C., Wang, S., 1986. Mesozoic and Cenozoic volcanic rocks from central and southern Tibet: ^{39}Ar–^{40}Ar dating, petrological characteristics and geodynamical significance. Earth Planet. Sci. Lett. 79, 281–302.

de Sigoyer, J., Chavagnac, V., Blichert-Toft, J., Villa, I.M., Luais, B., Guillot, S., Cosca, M., Mascle, G., 2000. Dating the Indian continental subduction and collisional thickening in the northwest Himalaya: Multichronology of the Tso Morari eclogites. Geology 28, 487–490.

Debon, F., Le Fort, P., Sheppard, S.M., Sonet, J., 1986. The four plutonic belts of the Transhimalaya–Himalaya: a chemical, mineralogical, isotopic, and chronological synthesis along a Tibet–Nepal section. J. Petrol. 27, 219–250.

Defant, M.J., Drummond, M.S., 1990. Derivation of some modern arc magmas by melting of young subducted lithosphere. Nature 347, 662–665.

Ding, L., 2003. Paleocene deep-water sediments and radiolarian faunas: Implications for evolution of Yarlung–Zangbu foreland basin, southern Tibet. Sci. China (D) 46, 84–96.

Ding, L., Kapp, P., Zhong, D., Deng, W., 2003. Cenozoic volcanism in Tibet: evidence for a transition from oceanic to continental subduction. J. Petrol. 44, 1833–1865.

Ding, L., Kapp, P., Wan, X.Q., 2005. Paleocene–Eocene record of ophiolite obduction and initial India–Asia collision, south central Tibet. Tectonic 24 2004TC001729.

Dong, G.C., Mo, X.X., Zhao, Z.D., Guo, T.Y., Wang, L.L., Chen, T., 2005. Geochronologic constraints on the magmatic underplating of the Gangdese belt in the India–Eurasia collision: evidence of SHRIMP II zircon U–Pb dating. Acta Geol. Sinica 79, 787–794.

Dong, Y.H., Xu, J.F., Zeng, Q.G., Wang, Q., Mao, G.Z., Li, J., 2006. Is there a Neo–Tethys' subduction record earlier than arc volcanic rocks in the Sangri Group (in Chinese with English abstract)? Acta Petrol. Sinica 22, 661–668.

Dunlap, W.J., Wysoczanski, R., 2002. Thermal evidence for early Cretaceous metamorphism in the Shyok suture zone and age of the Khardung volcanic rocks, Ladakh, India. J. Asian Earth Sci. 20, 481–490.

Dűrr, S.B., 1996. Provenance of Xigaze fore-arc basin clastic rocks (Cretaceous, south Tibet). Geol. Soc. Am. Bull. 108, 669–684.

Einsele, G., Liu, B., Dűrr, S., Frisch, W., Liu, G., Luterbacher, H.P., Ratschbacher, L., Ricken, W., Wendt, J., Wetzel, A., Yu, G., Zheng, H., 1994. The Xigaze forearc basin: Evolution and facies architecture (Cretaceous, Tibet). Sedi. Geol. 90, 1–32.

Garzanti, E., 2008. Comment on "When and where did India and Asia collide?" by Jonathan C. Aitchison, Jason R. Ali, and Aileen M. Davis. J. Geophys. Res. 113, B04411. doi:10.1029/2007JB005276.

Garzanti, E., Baud, A., Mascle, G., 1987. Sedimentary record of the northward flight of India and its collision with Eurasia (Ladakh Himalaya, India). Geodinamica Acta 1, 297–312.

Garzanti, E., Critelli, S., Ingersoll, R.V., 1996. Paleogeographic and paleotectonic evolution of the Himalayan Range as reflected by detrital modes of Tertiary sandstones and modern sands (Indus transects, India and Pakistan). Geol. Soc. Am. Bull. 108, 631–642.

Gehrels, G.E., DeCelles, P.G., Martin, A., Ojha, T.P., Pinhassi, G., Upreti, B.N., 2003. Initiation of the Himalayan orogen as an Early Paleozoic thin-skinned thrust belt. GSA Today 13 (9), 4–9.

Geng, Q.R., Pan, G.T., Wang, L.Q., Zhu, D.C., Liao, Z.L., 2006. Isotopic geochronology of the volcanic rocks from the Yeba Formation in the Gangdise zone, Xizang (in Chinese with English abstract). Sedi. Geol. Tethyan Geol. 26, 1–7.

Griffin, W.L., Pearson, N.J., Belousova, E., Jackson, S.E., van Achterbergh, E., O'Reilly, S.Y., Shee, S.R., 2000. The Hf isotope composition of cratonic mantle: LAM-MC-ICPMS analysis of zircon megacrysts in kimberlites. Geochim. Cosmochim. Acta 64, 133–147.

Griffin, W.L., Wang, X., Jackson, S.E., Pearson, N.J., O'Reilly, S.Y., Xu, X.S., Zhou, X.M., 2002. Zircon chemistry and magma mixing, SE China: In-situ analysis of Hf isotopes, Tonglu and Pingtan igneous complexes. Lithos 2002, 237–269.

Guo, Z.F., Wilson, M., Liu, J.Q., Mao, Q., 2007. Post-collisional adakites in south Tibet: products of partial melting of subduction-modified lower crust. Lithos 96, 205–224.

Harris, N.B.W., Xu, R., Lewis, C.L., Hawkeworth, C.J., Zhang, Y., 1988. Isotope geochemistry of the 1985 Tibet Geotraverse, Lhasa to Golmud. Phil Trans. R. Soc. Lond. A327, 263–285.

Harrison, T.M., Yin, A., Grove, M., Lovera, O.M., Ryerson, F.J., Zhou, X., 2000. The Zedong Window: a record of superposed Tertiary convergence in southeastern Tibet. J. Geophys. Res. 105, 19211–19230.

He, S.D., Kapp, P., DeCelles, P.G., Gehrels, G.E., Heizler, M., 2007. Cretaceous–Tertiary geology of the Gangdese Arc in the Linzhou area, southern Tibet. Tectonophysics 433, 15–37.

He, Z.H., Yang, D.M., Wang, T.W., Zheng, C.Q., 2005. SHRIMP U–Pb dating of zircons from two-mica granite in Baga area in Gangdise Belt (in Chinese with English abstract). J. Jilin Uni. (Earth Sci.) 35, 302–307.

He, Z.H., Yang, D.M., Zheng, C.Q., Wang, T.W., 2006. Isotopic dating of the Mamba granitoid in the Gangdise tectonic belt and its constraint on the subduction time of the Neotethys (in Chinese with English abstract). Geol. Rev. 52, 100–106.

Heuberger, S., Schaltegger, U., Burg, J.P., Villa, I.M., Frank, M., Dawood, H., Hussain, S., Zanchi, A., 2007. Age and isotopic constraints on magmatism along the Karakoram–Kohistan Suture Zone, NW Pakistan: evidence for subduction and continued convergence after India–Asia collision. Swiss J. Geosci. 100, 85–107.

Honegger, K.H., Dietrich, V., Frank, W., Gansser, A., Thommsdorf, M., Thommsdorf, K., 1982. Magmatism and metamorphism in the Ladakh Himalayas. Earth Planet. Sci. Lett. 60, 253–292.

Hou, Z.Q., Gao, Y.F., Qu, X.M., Rui, Z.Y., Mo, X.X., 2004. Origin of adakitic intrusives generated during mid-Miocene east^west extension in southern Tibet. Earth Planet. Sci. Lett. 220, 139–155.

Jackson, S.E., Pearson, N.J., Griffin, W.L., Belousova, E.A., 2004. The application of laser ablation-inductively coupled plasma-mass spectrometry (LA-ICP-MS) to *in situ* U–Pb zircon geochronology. Chem. Geol. 211, 47–69.

Jaeger, J.J., Courtillot, V., Tapponnier, P., 1989. Paleontological view of the ages of the Deccan Traps, the Cretaceous/Tertiary boundary, and the India–Asia collision. Geology 17, 316–319.

Jahn, B.M., Wu, F.Y., Hong, D.W., 2000. Important crustal growth in the Phanerozoic: Isotopic evidence of granitoids from East–Central Asia. Proc. Indian Acad. Sci. (Earth Planet. Sci.) 109, 5–20.

Jain, A.K., Singh, S., 2008. Tectonics of the southern Asian plate margin along the Karakoram shear zone: constraints from field observations and U–Pb SHRIMP ages. Tectonophysics 451, 186–205.

Jiang, W., Mo, X.X., Zhao, C.H., Guo, T.Y., Zhang, S.Q., 1999. Geochemistry of granitoid and its mafic microgranular enclave in Gangdise belt, Qinghai–Xizang Plateau (in Chinese with English abstract). Acta Petrol. Sinica 15, 89–97.

Kaneko, Y., Katayama, I., Yamanmoto, H., Misawa, K., Ishikawa, M., Rehman, H.U., Kausar, A.B., Shiraishi, K., 2003. Timing of Himalayan ultrahigh-pressure metamorphism:

sinking rate and subduction angle of the Indian continental crust beneath Asia. J. Metamorphic Geol. 21, 589–599.
Kapp, J.L.D., Harrison, T.M., Kapp, P., Grove, M., Lovera, O.M., Ding, L., 2005. The Nyainqentanglha Shan: a window into the tectonic, thermal, and geochemical evolution of the Lhasa block, southern Tibet. J. Geophys. Res. 110, B08413. doi:10.1029/2004JB003330.
Kemp, A.I.S., Hawkesworth, C.J., Paterson, B.A., Kinny, P.D., 2006. Episodic growth of the Gondwana supercontinent from hafnium and oxygen isotopes in zircon. Nature 439, 580–583.
Keto, L.S., Jacobsen, S.B., 1987. Nd and Sr isotopic variations of Early Paleozoic oceans. Earth Planet. Sci. Lett. 84, 27–41.
Kinny, P.D., Maas, R., 2003. Lu–Hf and Sm–Nd isotope systems in zircon. In: Hanchar, J.M., Hoskin, P.W.O. (Eds.), Zircon. Rev. Mineral. Geochem., vol. 53, pp. 327–341.
Klootwijk, C.T., Gee, J.S., Peirce, J.W., Smith, G.M., McFadden, P.L., 1992. An early India–Asia contact: paleomagnetic constraints from Ninetyeast Ridge, ODP Leg 121. Geology 20, 395–398.
Kohn, M., Parkinson, C.D., 2002. Petrologic case for Eocene slab breakoff during the Indo-Asian collision. Geology 30, 591–594.
Le Fort, P., 1988. Granites in the tectonic evolution of the Himalaya, Karakoram and southern Tibet. Phil. Trans. R. Soc. London 326 (A), 281–299.
Lee, H.Y., Chung, S.L., Wang, Y.B., Zhu, D.C., Yang, J.H., Song, B., Liu, D.Y., Wu, F.Y., 2007. Age, petrogenesis and geological significance of the Linzizong volcanic successions in the Linzhou basin, southern Tibet: evidence from zircon U–Pb dates and Hf isotopes (in Chinese with English abstract). Acta Petrol. Sinica 23, 493–500.
Lee, H.Y., Chung, S.L., Lo, C.H., Ji, J.Q., Lee, T.Y., Qian, Q., Zhang, Q., 2009. Eocene Neotethyan slab breakoff in southern Tibet inferred from the Linzizong volcanic record. Tectonophysics, in revision.
Lee, J., Hacker, B.R., Dinklage, W.S., Wang, Y., Gans, P., Calvert, A., Wan, J., Chen, W., Blythe, A.E., McClelland, W., 2000. Evolution of the Kangmar dome, southern Tibet: Structural, petrologic, and thermochronologic constraints. Tectonics 19, 872–895.
Leech, M.L., Singh, S., Jain, A.K., Klemperer, S.L., Manickavasagam, R.M., 2005. The onset of India-Asia continental collision: early, steep subduction required by the timing of UHP metamorphism in the western Himalaya. Earth Planet. Sci. Lett. 234, 83–97.
Li, C., Wang, T.W., Li, H.M., Zeng, Q.G., 2003. Discovery of Indosinian megaporphyritic granodiorite in the Gangdise area: evidence for the existence of paleo-Gangdise (in Chinese with English abstract). Geol. Bull. China 22, 364–366.
Li, G.B., Wan, X.Q., Liu, W.C., Liang, D.Y., Yun, H., 2005. Discovery of Paleogene marine stratum along the southern side of Yarlung–Zangbo suture zone and its implications in tectonics. Sci. China (D) 48, 647–661.
Liang, Y.H., Chung, S.L., Liu, D.Y., Xu, Y.G., Wu, F.Y., Yang, J.H., Wang, Y.B., Lo, C.H., 2008. Detrital zircon evidence from Burma for reorganization of the eastern Himalayan river system. Am. J. Sci. 308, 618–638.
Lin, W., Zhang, Y.Q., Liang, H.Y., Xie, Y.W., 2004. Petrochemistry and SHRIMP U–Pb zircon age of the Chongjiang ore-bearing porphyry in the Gangdese porpkyry copper belt (In Chinese with English abstract). Geochimica 33, 585–592.
Ludwig, K.R., 2003. User's Manual for Isoplot 3.0: A Geochronological Toolkit for Microsoft Excel. Berkeley Geochronology Center. Special publication 4, 1–71.
Maluski, G., Proust, F., Xiao, X.C., 1982. $^{39}Ar/^{40}Ar$ dating of the trans-Himalayan calc-alkaline magmatism of southern Tibet. Nature 298, 152–154.
McDermid, I.R.C., Aitchison, J.C., Davis, A.M., Harrison, T.M., Grove, M., 2002. The Zedong terrane: a Late Jurassic intra-oceanic magmatic arc within the Yarlung–Tsangpo suture zone, southeastern Tibet. Chem. Geol. 187, 267–277.
Miller, C.R., Schuster, U., Klotzli, W., Purtschellerr, F., 1999. Post-collisional potassic and ultrapotassic magmatism in SW Tibet: geochemical and Sr-Nd-Pb-O iIsotopic constraints for Mantle Source Characteristics and Petrogenesis. J. Petrol. 40, 1399–1424.
Mo, X.X., Zhao, Z.D., Deng, J.F., Dong, G.C., Zhou, S., Guo, T.Y., Zhang, S.Q., Wang, L.L., 2003. Response of volcanism to the India–Asia collision (in Chinese with English abstract). Earth Sci. Frontiers 10, 135–148.
Mo, X.X., Dong, G.C., Zhao, Z.D., Zhou, S., Wang, L.L., Qiu, R.Z., Zhang, F.Q., 2005a. Spatial and temporal distribution and characteristics of granitoids in the Gangdese, Tibet and implication for crustal growth and evolution (in Chinese with English abstract). Geol. J., China University 11, 281–290.
Mo, X.X., Dong, G.C., Zhao, Z.D., Guo, T.Y., Wang, L.L., Chen, T., 2005b. Timing of magma mixing in Gangdise magmatic belt during the India–Asia collision: zircon SHIRMP U–Pb dating. Acta Geologica Sinica 79, 66–76.
Mo, X.X., Hou, Z.Q., Niu, Y.L., Dong, G.C., Qu, X.M., Zhao, Z.D., Yang, Z.M., 2007. Mantle contributions to crustal thickening during continental collision: Evidence from Cenozoic igneous rocks in southern Tibet. Lithos 96, 225–242.
Mo, X.X., Niu, Y.L., Dong, G.C., Zhao, Z.D., Hou, Z.Q., Zhou, S., Ke, S., 2008. Contribution of syn-collisional felsic magmatism to continental crust growth: a case study of the Paleogene Linzizong volcanic succession in southern Tibet. Chem. Geol. 250, 49–67.
Mo, J.H., Liang, H.Y., Yu, H.X., Xie, Y.W., Zhang, Y.Q., 2006. Comparison of ELA-ICP-MS and SHRIMP U–Pb zircon ages of the Chongjiang and Qulong ore-bearing porphyrites in the Gangdese porphyry copper belt (in Chinese with English abstract). Geotect. Metallo. 30, 504–509.
Najman, Y., 2006. The detrital record of orogenesis: a review of approaches and techniques used in the Himalayan sedimentary basins. Earth Sci. Rev. 74, 1–72.
Pan, G.T., Mo, X.X., Hou, Z.Q., Zhu, D.C., Wang, L.Q., Li, G.M., Zhao, Z.D., Geng, Q.R., Liao, Z.L., 2006. Spatial–temporal framework of the Gangdese orogenic belt and its evolution (in Chinese with English abstract). Acta Petrol. Sinica 22, 521–533.
Patriat, P., Achache, J., 1984. Indian–Eurasia collision chronology has implications for crustal shortening and driving mechanism of plates. Nature 311, 615–621.
Patzelt, A., Li, H.M., Wang, J.D., Appel, E., 1996. Paleomagnetism of Cretaceous to Tertiary sediments from southern Tibet: evidence for the extent of the northern margin of India prior to the collision with Eurasia. Tectonophysics 259, 259–284.
Pedersen, R., Searle, M.P., Corfield, R.I., 2001. U–Pb zircon ages from the Spontang Ophiolite, Ladakh Himalaya. J. Geol. Soc. London 158, 513–520.
Prasad, G.V.R., Jaeger, J.J., Sahni, A., Gheerbrant, E., Khajuria, C.K., 1994. Eutherian mammals from the Upper Cretaceous (Maastrichtian) Intertrappean Beds of Naskal, Andhra Pradesh, India. J. Vert. Paleo. 14, 260–277.
Ravikant, V., Wu, F.Y., Ji, W.Q., in press. Zircon U–Pb and Hf isotopic constraints on petrogenesis of the Cretaceous–Tertiary granites in eastern Karakoram and Ladakh, India. Lithos. doi:10.1016/j.lithos.2008.12.013.
Richter, F.M., Lovera, O.M., Harrison, T.M., Copeland, P., 1991. Tibetan tectonics from $^{40}Ar/^{39}Ar$ analysis of a single K-feldspar sample. Earth Planet. Sci. Lett. 105, 266–278.
Rowley, D.B., 1996. Age of initiation of collision between India and Asia: a review of stratigraphic data. Earth Planet. Sci. Lett. 145, 1–13.
Rowley, D.B., 1998. Minimum age of initiation of collision between India and Asia north of Everest based on the subsidence history of the Zhepure Mountain section. J. Geol. 106, 229–235.
Rui, Z.Y., Hou, Z.Q., Qu, X.M., Zhang, L.S., Wang, L.S., Liu, Y.L., 2003. Metallogenetic epoch of the Gangdese porphyry copper belt and uplift of the Qinghai-Tibet Plateau (in Chinese with English abstract). Mineral Deposits 22, 217–225.
Schaltegger, U., Zeilinger, G., Frank, M., Burg, J.P., 2002. Multiple mantle sources during island arc magmatism: U–Pb and Hf isotopic evidence from the Kohistan arc complex, Pakistan. Terra Nova 14, 461–468.
Schärer, U., Hamet, J., Allègre, C.J., 1984a. The Transhimalaya Gangdese plutonism in the Ladakh region: a U–Pb and Rb–Sr study. Earth Planet. Sci. Lett. 67, 327–339.
Schärer, U., Xu, R.H., Allègre, C.J., 1984b. U–Pb geochronology of Gandese (Transhimalaya) plutonism in the Lhasa–Xigaze region Tibet, Earth Planet. Sci. Lett. 69, 311–320.
Schärer, U., Xu, R.H., Allègre, C.J., 1986. U–(Th) –Pb systematic and ages of Himalayan leucogranites, south Tibet. Earth Planet. Sci. Lett. 77, 35–48.
Scherer, E., Munker, C., Mezger, K., 2001. Calibration of the lutetium–hafnium clock. Science 293, 683–687.
Searle, M.P., Windley, B.F., Coward, M.P., Coward, M.P., Rex, A.J., Li, T.D., Xiao, X.C., Jan, M.Q., Thakur, V.C., Kumar, S., 1987. The closing of Tethys and the tectonics of the Himalaya. Geol. Soc. Am. Bull. 98, 678–701.
Searle, M., Corfield, R.I., Stephenson, B., McCarron, J., 1997. Structure of the North Indian continental margin in the Ladakh–Zanskar Himalayas: implications for the timing of obduction of the Spontang ophiolite, India–Asia collision and deformation events in the Himalaya, Geol. Mag. 134, 297–316.
Searle, M.P., Kahn, M.A., Fraser, J.E., Gough, S.J., 1999. The tectonic evolution of the Kohistan–Karakoram collision belt along the Karakoram Highway transect, north Pakistan. Tectonics 18, 929–949.
Searle, M.P., Noble, S.R., Cottle, J.M., Waters, D.J., Mitchell, A.H.G., Hlaing, T., Horstwood, M.S.A., 2007. Tectonic evolution of the Mogok metamorphic belt, Burma (Myanmar) constrained by U–Th–Pb dating of metamorphic and magmatic rocks. Tectonics 26, TC3014. doi:10.1029/2006TC002083.
Tonarini, S., Villa, I., Oberli, F., Meier, M., Spencer, D.A., Pognante, U., Ramsay, J.G., 1993. Eocene age of eclogite metamorphism in the Pakistan Himalaya: implications for India–Eurasian collision. Terra Nova, 5, 13–20.
Turner, S., Hawkesworth, C., Liu, J., Rogers, N., Kelley, S., van Calsteren, P., 1993. Timing of Tibetan uplift constrained by analysis of volcanic rocks. Nature 364, 50–54.
Turner, S., Arnaud, N., Liu, J., Rogers, N., Hawkesworth, C., Harris, N., Kelley, S., van Calsteren, P., Deng, W., 1996. Postcollision, shoshonitic volcanism on the Tibetan Plateau: implications for convective thinning of the lithosphere and the source of ocean island basalts. J. Petrol. 37, 45–71.
Upadhyay, R., Ram-Awatar, Kar1, R.K., Sinha, A.K., 2004. Palynological evidence for the Palaeocene evolution of the forearc basin, Indus Suture Zone, Ladakh, India. Terra Nova 16, 216–225.
Wang, L.L., Mo, X.X., Li, B., Dong, G.C., Zhao, Z.D., 2006. Geochronology and geochemistry of he ore-bearing porphyry in Qulong Cu (Mo) ore deposit, Tibet (in Chinese with English abstract). Acta Petrol. Sinica 22, 1001–1008.
Weinberg, R.F., Dunlap, W.J., 2000. Growth and deformation of the Ladakh Batholith, Northwest Himalayas: implications for timing of continental collision and origin of calc-alkaline batholiths. J. Geol. 108, 303–320.
Wen, D.R., Liu, D.Y., Chung, S.L., Chu, M.F., Ji, J.Q., Zhang, Q., Song, B., Lee, T.Y., Yeh, M.W., Lo, C.H., 2008. Zircon SHRIMP U–Pb ages of the Gangdese batholith and implications for Neotethyan subduction in southern Tibet. Chem. Geol. 252, 191–201.
Wiedenbeck, M., Alle, P., Corfu, F., Griffin, W.L., Meier, F., Oberli, F., Von Quadt, A., Roddick, J.C., Spiegel, W., 1995. Three natural zircon standards for U–Th–Pb, Lu–Hf, trace element, and REE analyses. Geostandards Newsletter. 19, 1–23.
Willems, H., Zhou, Z., Zhang, B., Grafe, K.U., 1996. Stratigraphy of the upper Cretaceous and Lower Tertiary strata in the Tethyan Himalayas of Tibet (Tingri area, China). Geol. Rundsch. 85, 723–754.
Williams, H.M., Turner, S., Kelley, S., Harris, N., 2001. Age and composition of dikes in Southern Tibet: new constraints on the timing of east–west extension and its relationship to postcollisional volcanism. Geology 29, 339–342.
Williams, H.M., Turner, S., Pearce, G.A., Kelley, S.P., Harris, N., 2004. Nature of the source regions for post-collisional, potassic magmatism in southern and northern Tibet from geochemical variations and inverse element modeling. J. Petrol. 45, 555–607.
Wu, F.Y., Yang, Y.H., Xie, L.W., Yang, J.H., Xu, P., 2006. Hf isotopic compositions of the standard zircons and baddeleyites used in U–Pb geochronology. Chem. Geol. 234, 105–126.
Wu, F.Y., Clift, P.D., Yang, J.H., 2007. Zircon Hf isotopic constraints on the sources of the Indus Molasse, Ladakh Himalaya, India. Tectonics 26, TC2014. doi:10.1029/2006TC002051.
Wu, F.Y., Ji, W.Q., Liu, C.Z., Chung, S.L., 2009. Detrital zircon U–Pb and Hf isotopic constraints from the Xigaze fore-arc basin, southern Tibet on the source provenance and Transhimalaya magmatic evolution. J. Geophys. Res., in revision.

Xia, B., Wei, Z.Q., Zhang, Y.Q., Xu, L.F., Li, J.F., Wang, Y.B., 2007. SHRIMP U–Pb zircon dating of granodiorite in the Kangrinboqe pluton in western Tibet, China and its geological implications. Geol. Bull. China 26, 1014–1017.

Xie, L.W., Zhang, Y.B., Zhang, H.H., Sun, J.F., Wu, F.Y., 2008. *In situ* simultaneous determination of trace elements, U–Pb and Lu–Hf isotopes in zircon and baddeleyite. Chinese Sci. Bull. 53, 1565–1573.

Yang, J.H., Wu, F.Y., Wilde, S.A., Xie, L.W., Yang, Y.H., Liu, X.M., 2007. Tracing magma mixing in granite genesis: *in situ* U–Pb dating and Hf-isotope analysis of zircons. Contrib. Mineral. Petrol. 153, 177–190.

Yang, J.S., Xu, Z.Q., Li, Z.L., Xu, X.Z., Li, T.F., Ren, Y.F., Li, H.Q., Chen, S.Y., Robinson, P.T., 2008a. Discovery of an eclogite belt in the Lhasa block, Tibet: a new border for Paleo-Tethys?. J. Asian Earth Sci. 34, 76–89.

Yang, Z.M., Hou, Z.Q., Xia, D.X., Song, Y.C., Li, Z., 2008b. Relationship between western porphyry and mineralization in Qulong copper deposit if Tibet and its enlightenment to further exploration (in Chinese with English abstract). Mineral Deposits 27, 28–36.

Yin, A., Harrison, T.M., 2000. Geologic evolution of the Himalayan–Tibetan orogen. Annu. Rev. Earth Planet. Sci. 28, 211–280.

Zhang, H.F., Harris, N., Parrish, R., Kelley, S., Zhang, L., Rogers, N., Argles, T., King, J., 2004. Causes and consequences of protracted melting of the mid-crust exposed in the North Himalayan antiform. Earth Planet. Sci. Lett. 228, 195–212.

Zhang, H.F., Xu, W.C., Guo, K.Q., Cai, H.M., Yuan, H.L., 2007a. Zircon U–Pb and Hf isotopic composition of deformed granite in the southern margin of the Gangdese belt, Tibet: evidence for early Jurassic subduction of Neo-Tethyan oceanic slab (in Chinese with English abstract). Acta Petrol. Acta 23, 1347–1353.

Zhang, H.F., Xu, W.C., Guo, J.Q., Zong, K.Q., Cai, H.M., Yuan, H.L., 2007b. Indosinian orogenesis of the Gangdese terrane: evidences from zircon U–Pb dating and petrogenesis of granitoids. Earth Sci. 32, 155–166.

Zhou, S., Mo, X.X., Dong, G.C., Zhao, Z.D., Qiu, R.Z., Guo, T.Y., Wang, L.L., 2004. ^{40}Ar–^{39}Ar geochronology of Cenozoic Linzizong volcanic rocks from Linzhou Basin, Tibet, China, and their geological implications. Chinese Sci. Bull. 49, 1970–1979.

Zhu, B., Kidd, W.S.F., Rowley, D., Currie, B., Shafique, N., 2005. Age of initiation of the India–Asia collision in the east–central Himalaya. J. Geol. 113, 265–285.

Zhu, D.C., Pan, G.T., Chung, S.L., Liao, Z.L., Wang, L.Q., Li, G.M., 2008. SHRIMP zircon age and geochemical constraints on the origin of Lower Jurassic volcanic rocks from the Yeba Formation, southern Gangdese, South Tibet. Inter. Geol. Rev. 50, 442–471.